

Near-field Electrodynamics of Atomically Doped Carbon Nanotubes^{*}

Igor V. Bondarev^{†,1}, Philippe Lambin[‡]

[†] *Institute for Nuclear Problems,
Belarusian State University,
Bobruiskaya Str.11, 220050 Minsk, BELARUS*

[‡] *Facultés Universitaires Notre-Dame de la Paix,
61 rue de Bruxelles, 5000 Namur, BELGIUM*

ABSTRACT

We develop a quantum theory of near-field electrodynamical properties of carbon nanotubes and investigate spontaneous decay dynamics of excited states and van der Waals attraction of the ground state of an atomic system close to a single-wall nanotube surface. Atomic spontaneous decay exhibits vacuum-field Rabi oscillations – a principal signature of strong atom-vacuum-field coupling. The strongly coupled atomic state is nothing but a 'quasi-1D cavity polariton'. Its stability is mainly determined by the atom-nanotube van der Waals interaction. Our calculations of the ground-state atom van der Waals energy performed within a universal quantum mechanical approach valid for both weak and strong atom-field coupling demonstrate the inapplicability of conventional weak-coupling-based van der Waals interaction models in a close vicinity of the nanotube surface.

Keywords: Carbon nanotubes, Quantum electrodynamics, Near-field effects

^{*} To be published in "*Nanotubes: New Research*", edited by F.Columbus (Nova Science, New York, 2005).

¹ Corresponding author. E-mail address: bondarev@tut.by

Contents

1	Introduction	3
2	Field Quantization Formalism	6
3	Total Hamiltonian in terms of the local photonic DOS	10
4	Spontaneous Decay Dynamics of an Excited Atomic State near a Carbon Nanotube	14
4.1	Qualitative Analysis	16
4.1.1	Markovian Approximation	16
4.1.2	Single-Resonance Approximation of the Local Photonic DOS	17
4.2	Numerical Results and Discussion	18
5	van der Waals Energy of a Ground-State Atom near a Carbon Nanotube	23
5.1	Qualitative Analysis	26
5.1.1	Weak Coupling Regime	26
5.1.2	Strong Coupling Regime	27
5.2	Numerical Results and Discussion	27
6	Conclusion	33
A	Two-level approximation	36
B	Green tensor and local photonic DOS	38
C	Relation of Eq. (70) with the Casimir–Polder formula	44

1 Introduction

Carbon nanotubes (CNs) are graphene sheets rolled-up into cylinders of approximately one nanometer in diameter. Extensive work carried out worldwide in recent years has revealed the intriguing physical properties of these novel molecular scale wires [1, 2]. Nanotubes have been shown to be useful for miniaturized electronic, mechanical, electromechanical, chemical and scanning probe devices and materials for macroscopic composites [3]. Important is that their intrinsic properties may be substantially modified in a controllable way by doping with extrinsic impurity atoms, molecules and compounds [4]. Recent successful experiments on encapsulation of single atoms into single-wall CNs [5] and their intercalation into single-wall CN bundles [4, 6], along with numerous studies of monoatomic gas absorption by the CN bundles (see [7] for a review), open routes for new challenging nanophotonics applications of atomically doped CN systems as various sources of coherent light emitted by dopant atoms. This, in turn, stimulates an in-depth theoretical analysis of near-field electrodynamical properties of atomically doped CNs. Of primary importance towards the nanophotonics applications are the problems of atomic spontaneous emission and atom-nanotube van der Waals (vdW) interactions. The problems are not only of applied but also of fundamental interest as they shed light on the peculiarities of the atom-electromagnetic-field interactions in low-dimensional dispersive and absorbing surroundings.

It has long been recognized that the spontaneous emission rate of an excited atom is not an immutable property, but that it can be modified by the atomic environment. Generally called the Purcell effect [8], the phenomenon is qualitatively explained by the fact that the local environment modifies the strength and distribution of the vacuum electromagnetic modes with which the atom can interact, resulting indirectly in the alteration of atomic spontaneous emission properties. The Purcell effect took on special significance recently in view of rapid progress in physics of nanostructures. Here, the control of spontaneous emission has been predicted to have a lot of useful applications, ranging from the improvement of existing devices (lasers, light emitting diodes) to such nontrivial functions as the emission of nonclassical states of light [9]. In particular, the enhancement of the spontaneous emission rate can be the first step towards the realization of a thresholdless laser [10] or a single photon source [11]. The possibility to control atomic spontaneous emission was shown theoretically for microcavities and microspheres [12, 13, 14], optical fibers [15], photonic crystals [16], semiconductor quantum dots [17]. Recent technological progress in fabrication of low-dimensional nanostructures has enabled the experimental investigation of spontaneous emission of single atoms [18] and semiconductor quantum dots [19, 20, 21] in microcavities, single molecules in photonic crystals [22], quantum dots in photonic crystal nanocavities [23, 24].

Typically, there may be two qualitatively different regimes of interaction of an excited atomic state with a vacuum electromagnetic field in the vicinity of the CN.

They are the weak coupling regime and the strong coupling regime [25]. The former is characterized by the monotonous exponential decay dynamics of the upper atomic state with the decay rate altered compared with the free-space value. The latter is, in contrast, strictly non-exponential and is characterized by reversible Rabi oscillations where the energy of the initially excited atom is periodically exchanged between the atom and the field. A theoretical analysis recently done [26, 27, 28] of spontaneous decay dynamics of excited atomic states near CNs has brought out fascinating peculiarities of the vacuum-field interactions in atomically doped CNs. The relative density of photonic states (DOS) near a CN effectively increases due to the presence of additional surface photonic states coupled with CN electronic quasiparticle excitations [26]. This causes an atom-vacuum-field coupling constant, which is proportional to the photonic DOS, to be very sensitive to the atom-CN-surface distance. If the atom is close enough to the CN surface and the atomic transition frequency is in the vicinity of a resonance of the photonic DOS, the system shows strong atom-vacuum-field coupling giving rise to rearrangement ("dressing") of atomic levels by the vacuum-field interaction [27, 28]. If the atom moves away from the CN surface, the atom-field coupling strength decreases, smoothly approaching the weak coupling regime at large atom-surface distances since the role of surface photonic states diminishes, causing the relative photonic DOS to decrease. This suggests strictly nonlinear atom-field coupling and a primary role of the distance-dependent (local) photonic DOS in the vicinity of the CN, so that conventional (weak-coupling) atom-field interaction models based upon standard vacuum quantum electrodynamics (QED) as well as those using the linear response theory (see [29, 30] for a review) are, in general, inapplicable for an atomic system in a close vicinity of a carbon nanotube.

The aforesaid is extremely important for a proper understanding the monoatomic gas absorption processes by the CNs, as they are those arising from the atom-nanotube vdW interaction, which, from a fundamental point of view, is the result of electrodynamic coupling between the polarization states of the interacting entities that originates from the vacuum fluctuations of an electromagnetic field. Modern *ab-initio* methods based on the density functional theory (DFT) let one study the cohesive and adsorption properties of single-wall CNs and CN bundles to an adequate level of accuracy [31]. For example, recent hydrogen [32, 33] and oxygen [34] adsorption DFT-based studies explore the CN gas-storage capacity and the nature of hole doping processes of the semiconducting CNs under oxygenation. However, DFT is known to be reliable in describing *short-range* electron correlation effects whereas the vdW energy is contributed by both short-range and long-range interactions [35]. The short-range contribution consists of the repulsive part and attractive part coming, respectively, from the overlap of core electrons on adjacent molecules and from the decrease in electron kinetic energy due to delocalization. The long-range contribution is known as the London energy [36] which originates from the (attractive) dispersion interaction of fluctuating dipoles and dominates the short-range contributions at distances larger than the equilibrium one. While adequate

in describing the first two contributions, DFT may fail in reproducing the long-range dispersion forces correctly, especially in graphitic structures as discussed in Ref. [35]. An alternative (classical) approach for computing the London dispersion energy is by summing up the empirical r^{-6} pair potentials with parameters fitted to experimental data, or for graphitic structures often taken from highly oriented pyrolytic graphite [37, 38].

We develop a quantum theory of near-field electrodynamical properties of atomically doped CNs and apply it to the study of atomic spontaneous emission and London-type dispersion atom-nanotube interaction (simply called the vdW interaction throughout this Chapter). Our theory is based on a unified macroscopic QED formalism developed for dispersing and absorbing media in Ref. [12, 13]. The formalism generalizes the standard macroscopic QED normal-mode technique by representing mode expansion in terms of a Green tensor of the (operator) Maxwell equations in which material dispersion and absorption are automatically included. In more detail, the Fourier-images of electric and magnetic fields are considered as quantum mechanical observables of corresponding electric and magnetic field operators. The latter ones satisfy the Fourier-domain operator Maxwell equations modified by the presence of a so-called operator noise current written in terms of a bosonic field operator and an imaginary dielectric permittivity. This operator is responsible for correct commutation relations of the electric and magnetic field operators in the presence of medium-induced absorption. The electric and magnetic field operators are then expressed in terms of a continuum set of operator bosonic fields by means of the convolution of the operator noise current with the electromagnetic field Green tensor of the system. The bosonic field operators create and annihilate single-quantum electromagnetic medium excitations. They are defined by their commutation relations and play the role of the fundamental dynamical variables in terms of which the Hamiltonian of the composed system "electromagnetic field + dissipative medium" is written in a standard secondly quantized form.

The Chapter is organized as follows. In Section 2, using the approach summarized above, we describe the general electromagnetic field quantization scheme and derive the total Hamiltonian for an atomic system (an atom or a molecule) nearby a single-wall carbon nanotube. The nanotube is considered as an infinitely long, infinitely thin, anisotropically conducting cylinder. Its surface conductivity is represented in terms of the π -electron dispersion law obtained in the tight-binding approximation with allowance made for the azimuthal electron momentum quantization and the axial electron momentum relaxation [39]. Only the axial conductivity is taken into account and the azimuthal one, being strongly suppressed by transverse depolarization fields [40, 41, 42, 43, 44], is neglected. In Section 3, based on the total Hamiltonian obtained in Section 2, we derive the simplified secondly quantized Hamiltonian representing the "atom-nanotube" coupled system in terms of two standard approximations. They are the electric dipole approximation and the atomic two-level approximation. This Hamiltonian generalizes that earlier ap-

plied for the atomic spontaneous decay analysis near spherical microcavities [12] and nanotubes [27, 28] in that the rotating wave approximation is not used and the diamagnetic term of the atom-field interaction is not neglected. This Hamiltonian is a starting point to derive an evolution equation for the population probability of the upper state (Section 4) and a van der Waals energy equation of the lower (ground) state of the two-level atomic system (Section 5) coupled with the CN modified vacuum electromagnetic field. The equations are represented in terms of the local photonic DOS and are valid for both strong and weak atom-field coupling. In Section 4, we demonstrate that when the atom is close enough to the nanotube surface and the atomic transition frequency is in the vicinity of a resonance of the local photonic DOS, the upper state of the coupled system decays via underdamped Rabi oscillations which are a principal signature of strong atom-vacuum-field coupling – the result recently detected for quasi-two-dimensional (2D) excitonic [45], inter-subband electronic [46] and quasi-0D excitonic [19, 21] transitions in semiconductor quantum microcavities as well as for quasi-0D excitonic transitions in photonic crystal nanocavities [23]. In Section 5, to take strong atom-field coupling into account in a correct way and thereby to advance in physical understanding the atom-nanotube vdW interactions deeper than simple analyzing empirical model potentials [35], we develop a universal quantum mechanical approach to the atom–nanotube vdW energy calculation. The approach was first suggested in Refs. [47, 48]. It is based on the perturbation theory for degenerate atomic levels (see, e.g., [49]), thereby allowing one to account for both strong and weak atom-vacuum-field coupling regimes in a simplest way. Within this approach, the ground-state atom vdW energy is given by the integral equation which reproduces a well-known perturbation theory result in the weak coupling regime. By solving it numerically, we demonstrate the inapplicability of conventional weak-coupling-based vdW interaction models in a close vicinity of the nanotube surface. A summary and conclusions are given in Section 6.

2 Field Quantization Formalism

The quantum theory of the near-field electrodynamical properties of carbon nanotubes involves an electromagnetic field quantization procedure in the presence of dispersing and absorbing bodies. Such a procedure faces difficulties similar to those in quantum optics of 3D Kramers-Kronig dielectric media where the canonical quantization scheme commonly used does not work since, because of absorption, corresponding operator Maxwell equations become non-Hermitian [50]. As a consequence, their solutions cannot be expanded in power orthogonal modes and the concept of modes itself becomes more subtle. We, therefore, use a unified macroscopic QED approach developed in Refs. [12, 13]. In this approach, the Fourier-images of electric and magnetic fields are considered as quantum mechanical observables of corresponding electric and magnetic field operators. The latter ones satisfy the Fourier-domain operator Maxwell equations modified by the presence of a so-called operator

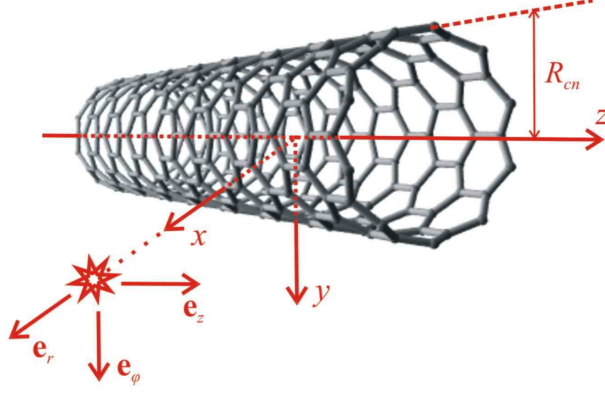


Figure 1: The geometry of the problem.

noise current density $\hat{\mathbf{J}}(\mathbf{r}, \omega)$ written in terms of a 3D vector bosonic field operator $\hat{\mathbf{f}}(\mathbf{r}, \omega)$ and a medium dielectric tensor $\epsilon(\mathbf{r}, \omega)$ (supposed to be diagonal) as¹

$$\hat{J}_i(\mathbf{r}, \omega) = \frac{\omega}{2\pi} \sqrt{\hbar \text{Im} \epsilon_{ii}(\mathbf{r}, \omega)} \hat{f}_i(\mathbf{r}, \omega), \quad i = 1, 2, 3. \quad (1)$$

This operator is responsible for correct commutation relations of the electric and magnetic field operators in the presence of medium-induced absorption. In this formalism, the electric and magnetic field operators are expressed in terms of a continuum set of the 3D vector bosonic fields $\hat{\mathbf{f}}(\mathbf{r}, \omega)$ by means of the convolution over \mathbf{r} of the current (1) with the classical electromagnetic field Green tensor of the system. The bosonic field operators $\hat{f}_i^\dagger(\mathbf{r}, \omega)$ and $\hat{f}_i(\mathbf{r}, \omega)$ create and annihilate single-quantum electromagnetic medium excitations. They are defined by their commutation relations

$$\begin{aligned} [\hat{f}_i(\mathbf{r}, \omega), \hat{f}_j^\dagger(\mathbf{r}', \omega')] &= \delta_{ij} \delta(\mathbf{r} - \mathbf{r}') \delta(\omega - \omega'), \\ [\hat{f}_i(\mathbf{r}, \omega), \hat{f}_j(\mathbf{r}', \omega')] &= [\hat{f}_i^\dagger(\mathbf{r}, \omega), \hat{f}_j^\dagger(\mathbf{r}', \omega')] = 0 \end{aligned} \quad (2)$$

and play the role of the fundamental dynamical variables in terms of which the Hamiltonian of the composed system "electromagnetic field + dissipative medium" is written in a standard secondly quantized form as

$$\hat{H} = \int_0^\infty d\omega \hbar \omega \int d\mathbf{r} \hat{\mathbf{f}}^\dagger(\mathbf{r}, \omega) \cdot \hat{\mathbf{f}}(\mathbf{r}, \omega). \quad (3)$$

Consider a neutral atomic system (an atom or a molecule) with its centre-of-mass positioned at the point \mathbf{r}_A near an infinitely long single-wall CN. Since the problem has a cylindric symmetry, assign the orthonormal cylindric basis $\{\mathbf{e}_r, \mathbf{e}_\varphi, \mathbf{e}_z\}$ with

¹We use Gaussian units. Conversion tables to SI can be found elsewhere (see, e.g., [51]).

\mathbf{e}_z directed along the nanotube axis and $\mathbf{r}_A = r_A \mathbf{e}_r = \{r_A, 0, 0\}$ (see Fig. 1). For carbon nanotubes, their strong transverse depolarization along with transverse electron momentum quantization allow one to neglect the azimuthal current and radial polarizability [39, 40, 41, 42, 43, 44], in which case the dielectric tensor components ϵ_{rr} and $\epsilon_{\varphi\varphi}$ are identically equal to unit. The component ϵ_{zz} is caused by the CN longitudinal polarizability and is responsible for the axial surface current parallel to the \mathbf{e}_z vector. This current may be represented in terms of the 1D bosonic field operators by analogy with Eq. (1). Indeed, taking into account the dimensionality conservation in passing from bulk to a monolayer in Eq. (3) and using a simple Drude relation [41]

$$\sigma_{zz}(\mathbf{R}, \omega) = -i\omega \frac{\epsilon_{zz}(\mathbf{R}, \omega) - 1}{4\pi S \rho_T}, \quad (4)$$

where $\mathbf{R} = \{R_{cn}, \phi, Z\}$ is the radius-vector of an arbitrary point of the CN surface, R_{cn} is the radius of the CN, $\sigma_{zz}(\mathbf{R}, \omega)$ is the CN surface axial conductivity per unit length, S is the area of a single nanotube, ρ_T is the cubic density of the tubule, one immediately has from Eq. (1)

$$\hat{\mathbf{J}}(\mathbf{R}, \omega) = \sqrt{\frac{\hbar\omega \text{Re}\sigma_{zz}(\mathbf{R}, \omega)}{\pi}} \hat{f}(\mathbf{R}, \omega) \mathbf{e}_z \quad (5)$$

with $\hat{f}(\mathbf{R}, \omega)$ being the 1D bosonic field operator defined on the CN surface. The operators $\hat{f}^\dagger(\mathbf{R}, \omega)$ and $\hat{f}(\mathbf{R}, \omega)$ satisfy the commutation relations (2) on the surface of the CN. They create and annihilate the single-quantum bosonic-type electromagnetic medium excitation of the frequency ω at the point \mathbf{R} of the CN surface.

We are now in a position to define the Hamiltonian of the system. Following the general macroscopic QED approach in the presence of absorbing and dispersive media [13], we introduce the total nonrelativistic Hamiltonian of an atomic system interacting with a CN modified quantized vacuum electromagnetic field in the form

$$\begin{aligned} \hat{H} = & \int_0^\infty d\omega \hbar\omega \int d\mathbf{R} \hat{f}^\dagger(\mathbf{R}, \omega) \hat{f}(\mathbf{R}, \omega) \\ & + \sum_i \frac{1}{2m_i} \left[\hat{\mathbf{p}}_i - \frac{q_i}{c} \hat{\mathbf{A}}(\mathbf{r}_A + \hat{\mathbf{r}}_i) \right]^2 + \frac{1}{2} \int d\mathbf{r} \hat{\rho}_A(\mathbf{r}) \hat{\varphi}_A(\mathbf{r}) + \int d\mathbf{r} \hat{\rho}_A(\mathbf{r}) \hat{\varphi}(\mathbf{r}), \end{aligned} \quad (6)$$

where m_i , q_i , $\hat{\mathbf{r}}_i$ and $\hat{\mathbf{p}}_i$ are, respectively, the masses, charges, coordinates (relative to \mathbf{r}_A) and momenta of the particles constituting the atomic subsystem. The first term of the Hamiltonian describes the quantized *medium-assisted* vacuum electromagnetic field in the presence of the CN. The second and the third terms represent the kinetic energy of the charged particles and their mutual Coulomb interaction, respectively, with

$$\hat{\varphi}_A(\mathbf{r}) = \int d\mathbf{r}' \frac{\hat{\rho}_A(\mathbf{r}')}{|\mathbf{r} - \mathbf{r}'|} \quad (7)$$

being the scalar potential of the charged particles distributed with the density $\hat{\rho}_A(\mathbf{r}) = \sum_i q_i \delta(\mathbf{r} - \mathbf{r}_A - \hat{\mathbf{r}}_i)$ in the atomic subsystem. The last term of the Hamiltonian accounts for the Coulomb interaction of the particles with the CN. The vector potential $\hat{\mathbf{A}}$ and the scalar potential $\hat{\phi}$ of the CN modified electromagnetic field are given for an arbitrary $\mathbf{r} = \{r, \varphi, z\}$ in the Schrödinger picture by

$$\hat{\mathbf{A}}(\mathbf{r}) = \int_0^\infty d\omega \frac{c}{i\omega} \hat{\underline{\mathbf{E}}}^\perp(\mathbf{r}, \omega) + \text{h.c.}, \quad (8)$$

$$-\nabla \hat{\phi}(\mathbf{r}) = \int_0^\infty d\omega \hat{\underline{\mathbf{E}}}^\parallel(\mathbf{r}, \omega) + \text{h.c.}, \quad (9)$$

where

$$\hat{\underline{\mathbf{E}}}^{\perp(\parallel)}(\mathbf{r}, \omega) = \int d\mathbf{r}' \hat{\boldsymbol{\delta}}^{\perp(\parallel)}(\mathbf{r} - \mathbf{r}') \cdot \hat{\underline{\mathbf{E}}}(\mathbf{r}', \omega) \quad (10)$$

is the transverse (longitudinal) electric field operator with

$$\delta_{\alpha\beta}^\parallel(\mathbf{r}) = -\nabla_\alpha \nabla_\beta \frac{1}{4\pi r} \quad (11)$$

and

$$\delta_{\alpha\beta}^\perp(\mathbf{r}) = \delta_{\alpha\beta} \delta(\mathbf{r}) - \delta_{\alpha\beta}^\parallel(\mathbf{r}) \quad (12)$$

being the longitudinal and transverse dyadic δ -functions, respectively, and $\hat{\underline{\mathbf{E}}}$ representing the total electric field operator which satisfies the following set of Fourier-domain Maxwell equations

$$\nabla \times \hat{\underline{\mathbf{E}}}(\mathbf{r}, \omega) = ik \hat{\underline{\mathbf{H}}}(\mathbf{r}, \omega), \quad (13)$$

$$\nabla \times \hat{\underline{\mathbf{H}}}(\mathbf{r}, \omega) = -ik \hat{\underline{\mathbf{E}}}(\mathbf{r}, \omega) + \frac{4\pi}{c} \hat{\underline{\mathbf{I}}}(\mathbf{r}, \omega). \quad (14)$$

Here, $\hat{\underline{\mathbf{H}}}$ stands for the magnetic field operator, $k = \omega/c$, and

$$\hat{\underline{\mathbf{I}}}(\mathbf{r}, \omega) = \int d\mathbf{R} \delta(\mathbf{r} - \mathbf{R}) \hat{\underline{\mathbf{J}}}(\mathbf{R}, \omega) = 2\hat{\underline{\mathbf{J}}}(R_{cn}, \varphi, z, \omega) \delta(r - R_{cn}), \quad (15)$$

is the exterior operator current density [with $\hat{\underline{\mathbf{J}}}(\mathbf{R}, \omega)$ defined by Eq. (5)] associated with the presence of the CN.

From Eqs. (13)-(15) in view of Eq. (5), it follows that

$$\hat{\underline{\mathbf{E}}}(\mathbf{r}, \omega) = i \frac{4\pi}{c} k \int d\mathbf{R} \mathbf{G}(\mathbf{r}, \mathbf{R}, \omega) \cdot \hat{\underline{\mathbf{J}}}(\mathbf{R}, \omega) \quad (16)$$

[and $\hat{\underline{\mathbf{H}}} = (ik)^{-1} \nabla \times \hat{\underline{\mathbf{E}}}$ accordingly], where \mathbf{G} is the Green tensor of the classical electromagnetic field in the vicinity of the CN. The Green tensor components satisfy the equation

$$\sum_{\alpha=r,\varphi,z} (\nabla \times \nabla \times - k^2)_{z\alpha} G_{\alpha z}(\mathbf{r}, \mathbf{R}, \omega) = \delta(\mathbf{r} - \mathbf{R}), \quad (17)$$

together with the radiation conditions at infinity and the boundary conditions on the CN surface. The set of Eqs. (6)-(17) forms a closed electromagnetic field quantization formalism in the presence of dispersing and absorbing media which meets all the basic requirements of the standard quantum electrodynamics [13]. All the information about medium, which is a carbon nanotube in our case, is contained in the Green tensor \mathbf{G} via the CN surface axial conductivity σ_{zz} in Eq. (5) which comes into play when \mathbf{G} is imposed the boundary conditions on the CN surface. The classical electromagnetic field Green tensor of the "atom-nanotube" system is derived in Appendix B.

Assuming further that the atomic subsystem is sufficiently localized in space, so that the long-wavelength approximation applies, one can expand the field operators $\hat{\mathbf{A}}(\mathbf{r})$ and $\hat{\varphi}(\mathbf{r})$ in the Hamiltonian (6) around the atomic center of mass position \mathbf{r}_A and only keep the leading non-vanishing terms of the expansions. Then, under the condition of the Coulomb gauge $[\hat{\mathbf{p}}_i, \hat{\mathbf{A}}] = 0$, one arrives at the approximate total Hamiltonian of the form

$$\hat{H} = \hat{H}_F + \hat{H}_A + \hat{H}_{AF}^{(1)} + \hat{H}_{AF}^{(2)}, \quad (18)$$

where

$$\hat{H}_F = \int_0^\infty d\omega \hbar\omega \int d\mathbf{R} \hat{f}^\dagger(\mathbf{R}, \omega) \hat{f}(\mathbf{R}, \omega), \quad (19)$$

$$\hat{H}_A = \sum_i \frac{\hat{\mathbf{p}}_i^2}{2m_i} + \sum_{i < j} \frac{q_i q_j}{|\mathbf{r}_i - \mathbf{r}_j|}, \quad (20)$$

$$\hat{H}_{AF}^{(1)} = - \sum_i \frac{q_i}{m_i c} \hat{\mathbf{p}}_i \cdot \hat{\mathbf{A}}(\mathbf{r}_A) + \hat{\mathbf{d}} \cdot \nabla \hat{\varphi}(\mathbf{r}_A), \quad (21)$$

$$\hat{H}_{AF}^{(2)} = \sum_i \frac{q_i^2}{2m_i c^2} \hat{\mathbf{A}}^2(\mathbf{r}_A) \quad (22)$$

are, respectively, the Hamiltonian of the vacuum electromagnetic field modified by the presence of the CN, the Hamiltonian of the atomic subsystem, and the electric dipole approximation for the Hamiltonian of the atom-field interaction (separated into two contributions according to their role in the vdW energy – see below) with $\hat{\mathbf{d}} = \sum_i q_i \hat{\mathbf{r}}_i$ being the electric dipole moment operator of the atomic subsystem.

3 Total Hamiltonian in terms of the local photonic DOS

Starting from Eqs. (18)-(22) and using Eqs. (8)-(12), (16) and (5), one obtains the following two-level approximation for the total Hamiltonian of the system (see Appendix A)

$$\hat{\mathcal{H}} = \hat{\mathcal{H}}_0 + \hat{\mathcal{H}}_{int}, \quad (23)$$

where the first term stands for the unperturbed Hamiltonian given by

$$\hat{\mathcal{H}}_0 = \hat{H}_F + \hat{\mathcal{H}}_A \quad (24)$$

with \hat{H}_F being the Hamiltonian (19) of the CN modified field and

$$\hat{\mathcal{H}}_A = \frac{\hbar\tilde{\omega}_A}{2} \hat{\sigma}_z \quad (25)$$

representing the 'effective' unperturbed two-level atomic subsystem, and the second term stands for their interaction given by

$$\hat{\mathcal{H}}_{int} = \int_0^\infty d\omega \int d\mathbf{R} [g^{(+)}(\mathbf{r}_A, \mathbf{R}, \omega) \hat{\sigma}^\dagger - g^{(-)}(\mathbf{r}_A, \mathbf{R}, \omega) \hat{\sigma}] \hat{f}(\mathbf{R}, \omega) + \text{h.c.} \quad (26)$$

Here, the Pauli operators

$$\begin{aligned} \hat{\sigma} &= |l\rangle\langle u|, \quad \hat{\sigma}^\dagger = |u\rangle\langle l|, \quad \hat{\sigma}_z = |u\rangle\langle u| - |l\rangle\langle l|, \\ |u\rangle\langle u| + |l\rangle\langle l| &= \hat{I}, \end{aligned} \quad (27)$$

describe electric dipole transitions between the two atomic states, upper $|u\rangle$ and lower $|l\rangle$, separated by the transition frequency ω_A . This 'bare' transition frequency is modified by the interaction (22) which, being independent of the atomic dipole moment, does not contribute to mixing the $|u\rangle$ and $|l\rangle$ states, giving rise, however, to the new *renormalized* transition frequency

$$\tilde{\omega}_A = \omega_A \left[1 - \frac{2}{(\hbar\omega_A)^2} \int_0^\infty d\omega \int d\mathbf{R} |g^\perp(\mathbf{r}_A, \mathbf{R}, \omega)|^2 \right] \quad (28)$$

in the 'effective' atomic Hamiltonian (25). On the contrary, the interaction (21), being dipole moment dependent, mixes the $|u\rangle$ and $|l\rangle$ states, yielding the perturbation Hamiltonian (26) with the (dipole) interaction matrix elements of the form

$$g^{(\pm)}(\mathbf{r}_A, \mathbf{R}, \omega) = g^\perp(\mathbf{r}_A, \mathbf{R}, \omega) \pm \frac{\omega}{\omega_A} g^\parallel(\mathbf{r}_A, \mathbf{R}, \omega), \quad (29)$$

where

$$g^{\perp(\parallel)}(\mathbf{r}_A, \mathbf{R}, \omega) = -i \frac{4\omega_A}{c^2} d_z \sqrt{\pi \hbar \omega \text{Re} \sigma_{zz}(\mathbf{R}, \omega)}^{\perp(\parallel)} G_{zz}(\mathbf{r}_A, \mathbf{R}, \omega) \quad (30)$$

with $d_z = \langle l | \hat{d}_z | u \rangle = \langle u | \hat{d}_z | l \rangle$ being the matrix element of the atomic dipole moment z -component and

$$^{\perp(\parallel)} G_{zz}(\mathbf{r}_A, \mathbf{R}, \omega) = \int d\mathbf{r} \delta_{zz}^{\perp(\parallel)}(\mathbf{r}_A - \mathbf{r}) G_{zz}(\mathbf{r}, \mathbf{R}, \omega) \quad (31)$$

representing the field Green tensor zz -component transverse (longitudinal) with respect to the first variable. This is the only Green tensor component we have to

take account of. All the other components can be safely neglected, because our model neglects the azimuthal current and radial polarizability of the CN from the very outset [see the discussion above Eq. (4)].

Matrix elements (29) and (30) have the following properties (Appendix B)

$$\int d\mathbf{R} |g^{\perp(\parallel)}(\mathbf{r}_A, \mathbf{R}, \omega)|^2 = \frac{(\hbar\omega_A)^2}{2\pi\omega^2} \Gamma_0(\omega) \xi^{\perp(\parallel)}(\mathbf{r}_A, \omega) \quad (32)$$

and

$$\int d\mathbf{R} |g^{(\pm)}(\mathbf{r}_A, \mathbf{R}, \omega)|^2 = \frac{(\hbar\omega_A)^2}{2\pi\omega^2} \Gamma_0(\omega) \left[\xi^{\perp}(\mathbf{r}_A, \omega) + \left(\frac{\omega}{\omega_A} \right)^2 \xi^{\parallel}(\mathbf{r}_A, \omega) \right]. \quad (33)$$

Here, $\xi^{\perp}(\mathbf{r}_A, \omega)$ and $\xi^{\parallel}(\mathbf{r}_A, \omega)$ are the transverse and longitudinal *local* (position-dependent) photonic DOS functions defined by

$$\xi^{\perp(\parallel)}(\mathbf{r}_A, \omega) = \frac{\text{Im}^{\perp(\parallel)} G_{zz}^{\perp(\parallel)}(\mathbf{r}_A, \mathbf{r}_A, \omega)}{\text{Im} G_{zz}^0(\mathbf{r}_A, \mathbf{r}_A, \omega)}, \quad (34)$$

where

$${}^{\perp(\parallel)} G_{zz}^{\perp(\parallel)}(\mathbf{r}_A, \mathbf{r}_A, \omega) = \int d\mathbf{r} d\mathbf{r}' \delta_{zz}^{\perp(\parallel)}(\mathbf{r}_A - \mathbf{r}) G_{zz}(\mathbf{r}, \mathbf{r}', \omega) \delta_{zz}^{\perp(\parallel)}(\mathbf{r}' - \mathbf{r}_A) \quad (35)$$

is the Green tensor zz -component transverse (longitudinal) with respect to both coordinate variables,

$$\text{Im} G_{zz}^0(\mathbf{r}_A, \mathbf{r}_A, \omega) = \frac{\omega}{6\pi c} \quad (36)$$

is the vacuum imaginary Green tensor zz -component [52], and

$$\Gamma_0(\omega) = \frac{8\pi d_z^2 \omega^2}{3\hbar c^2} \text{Im} G_{zz}^0(\mathbf{r}_A, \mathbf{r}_A, \omega) = \frac{4d_z^2 \omega^3}{3\hbar c^3} \quad (37)$$

is the atomic spontaneous decay rate for the z -oriented atomic dipole in vacuum, taken at an arbitrary frequency ω [53, 54].

Note that the transverse and longitudinal imaginary Green tensor components in Eq. (34) can be written as

$$\text{Im}^{\perp} G_{zz}^{\perp} = \text{Im} G_{zz}^0 + \text{Im}^{\perp} \overline{G}_{zz}^{\perp}, \quad (38)$$

$$\text{Im}^{\parallel} G_{zz}^{\parallel} = \text{Im}^{\parallel} \overline{G}_{zz}^{\parallel} \quad (39)$$

with ${}^{\perp(\parallel)} \overline{G}_{zz}^{\perp(\parallel)}$ representing the "pure" CN contribution to the total imaginary Green tensor. The longitudinal imaginary Green tensor in Eq. (39) is totally contributed by a (longitudinal) CN static polarization field and, therefore, does not contain the vacuum term which is the transverse one by its definition as there are no polarization

Coulomb sources in vacuum [51, 52]. Thus, Eq. (34) may, in view of Eqs. (38) and (39), be rewritten in the form

$$\xi^\perp(\mathbf{r}_A, \omega) = 1 + \bar{\xi}^\perp(\mathbf{r}_A, \omega), \quad (40)$$

$$\xi^\parallel(\mathbf{r}_A, \omega) = \bar{\xi}^\parallel(\mathbf{r}_A, \omega), \quad (41)$$

where the \mathbf{r}_A -dependent terms come from the presence of the CN. For $r_A > R_{cn}$, they are explicitly given by (Appendix B)

$$\bar{\xi}^\perp(\mathbf{r}_A, x) = \frac{3}{\pi} \text{Im} \sum_{p=-\infty}^{\infty} \int_C \frac{dy s(R_{cn}, x) v(y)^4 I_p^2[v(y)u(R_{cn})x] K_p^2[v(y)u(r_A)x]}{1 + s(R_{cn}, x) v(y)^2 I_p[v(y)u(R_{cn})x] K_p[v(y)u(R_{cn})x]}, \quad (42)$$

$$\bar{\xi}^\parallel(\mathbf{r}_A, x) = \frac{3}{\pi} \text{Im} \sum_{p=-\infty}^{\infty} \int_C \frac{dy s(R_{cn}, x) y^2 v(y)^2 I_p^2[v(y)u(R_{cn})x] K_p^2[v(y)u(r_A)x]}{1 + s(R_{cn}, x) v(y)^2 I_p[v(y)u(R_{cn})x] K_p[v(y)u(R_{cn})x]}, \quad (43)$$

where

$$x = \frac{\hbar}{2\gamma_0} \omega \quad (44)$$

is the dimensionless frequency with $\gamma_0 = 2.7$ eV being the carbon nearest neighbor hopping integral [55] appearing in the CN surface axial conductivity in Eq. (5), I_p and K_p are the modified cylindric Bessel functions, $v(y) = \sqrt{y^2 - 1}$, $u(r) = 2\gamma_0 r / \hbar c$, and $s(R_{cn}, x) = 2i\alpha u(R_{cn})x \bar{\sigma}_{zz}(R_{cn}, x)$ with $\bar{\sigma}_{zz} = 2\pi\hbar\sigma_{zz}/e^2$ being the dimensionless CN surface conductivity per unit length and $\alpha = e^2/\hbar c = 1/137$ representing the fine-structure constant. The integration contour C runs along the real axis of the complex plane and envelopes the branch points $y = \pm 1$ of the function $v(y)$ in the integrands from below and from above, respectively. For $r_A < R_{cn}$, Eqs. (42) and (43) are modified by a simple replacement $r_A \leftrightarrow R_{cn}$ in the Bessel function arguments in the numerators of the integrands. Note the divergence of the local photonic DOS functions $\bar{\xi}^{\perp(\parallel)}(\mathbf{r}_A, x)$ at $r_A = R_{cn}$, i. e. when the atom is located right on the CN surface. Mathematically, this comes from the logarithmic divergence of the Bessel function K_0 at small arguments (see, e.g., [56]), yielding the divergent product $I_0 K_0$ and, as a consequence, the divergent integrands in Eqs. (42) and (43), if and only if the arguments of the functions I_0 and K_0 in the numerator of the integrand vanish simultaneously. Physically, the point is that the CN dielectric tensor longitudinal component ϵ_{zz} [which, according to Eqs. (4), (5) and (16) is responsible for the surface axial conductivity σ_{zz} in Eqs. (42) and (43)] is obtained as a result of a standard procedure of *physical* averaging a local electromagnetic field over the two spatial directions in the graphene plane [57]. Such averaging does not assume extrinsic atoms on the graphene surface. To take them into consideration the averaging procedure must be modified. Thus, the applicability domain of our model is restricted by the condition

$$|r_A - R_{cn}| > a, \quad (45)$$

where $a = 1.42 \text{ \AA}$ is the graphene interatomic distance [55].

Eqs. (23)–(30) represent the total secondly quantized Hamiltonian of an atomic system interacting with the electromagnetic field in the vicinity of the carbon nanotube. In deriving this Hamiltonian, there were only two standard approximations done. They are the electric dipole approximation and the two-level approximation. The rotating wave approximation commonly used was not applied, and the (diamagnetic) $\hat{\mathbf{A}}^2$ -term of the atom-field interaction [Eq. (22)] was not neglected. The latter two approximations are justified in analyzing an atomic state evolution due to *real* dipole transitions to the nearest states (shown schematically in Fig. 2) [25], described for two-level systems by the $g^{(+)}$ -terms of the Hamiltonian (26). They are, however, inappropriate in calculating the energy, where the initial energy level is being shifted due to the perturbation caused by *virtual* dipole transitions via intermediate atomic states (see Fig. 6 in Section 5), so that the system always remains in the initial state and the terms neglected contribute to the level shift to the same order of magnitude. For two-level systems, this is described by $g^{(-)}$ -terms of the Hamiltonian (26) (usually neglected within the rotating wave approximation) together with the atomic transition frequency (28) renormalized due to the (usually discarded) $\hat{\mathbf{A}}^2$ -term of the atom-field interaction.

4 Spontaneous Decay Dynamics of an Excited Atomic State near a Carbon Nanotube

When the atom is initially in the upper state and the field subsystem is in vacuum (see Fig. 2), the time-dependent wave function of the whole system can be written as

$$|\psi(t)\rangle = C_u(t) e^{-i(\tilde{\omega}_A/2)t} |u\rangle |\{0\}\rangle + \int d\mathbf{R} \int_0^\infty d\omega C_l(\mathbf{R}, \omega, t) e^{-i(\omega - \tilde{\omega}_A/2)t} |l\rangle |\{1(\mathbf{R}, \omega)\}\rangle, \quad (46)$$

where $|\{0\}\rangle$ is the vacuum state of the field subsystem, $|\{1(\mathbf{R}, \omega)\}\rangle$ is its excited state where the field is in a single-quantum Fock state, C_u and C_l are the population probability amplitudes of the upper state and lower state of the *whole* system, respectively. The function (46) accounts for the lower state degeneracy with respect to \mathbf{R} as well as its possible degeneracy with respect to ω when $\omega \sim \tilde{\omega}_A$ as is seen in Fig. 2.

The time-dependent Schrödinger equation with the Hamiltonian (23)–(26) and the wave function (46) yields the following evolution law for the population probability amplitude C_u of the upper state

$$C_u(t) = 1 + \int_0^t K(t-t') C_u(t') dt', \quad (47)$$

$$K(t-t') = \frac{1}{\hbar^2} \int_0^\infty d\omega \frac{e^{-i(\omega - \tilde{\omega}_A)(t-t')} - 1}{i(\omega - \tilde{\omega}_A)} \int d\mathbf{R} |g^{(+)}(\mathbf{r}_A, \mathbf{R}, \omega)|^2. \quad (48)$$

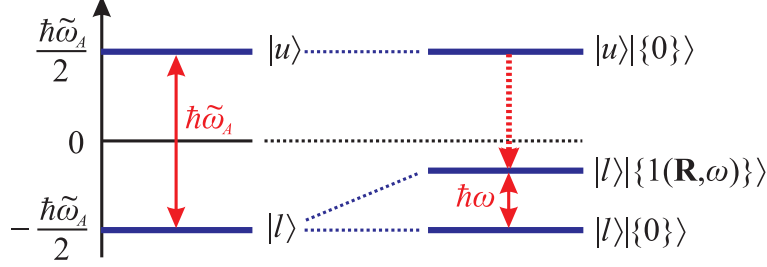


Figure 2: Schematic of the energy levels of the "atom-nanotube" coupled system in the problem of the spontaneous decay. On the left are the unperturbed atomic levels given by the Hamiltonian (25), on the right are the levels of the coupled system. The relevant real transition of the system is shown by the vertical dashed arrow. See Eqs. (53) and (44) for $\tilde{\omega}_A$.

This, upon recalling Eqs. (33), (40), (41) and (44) and introducing the dimensionless time

$$\tau = \frac{2\gamma_0}{\hbar} t, \quad (49)$$

reduces in dimensionless variables to

$$C_u(\tau) = 1 + \int_0^\tau K(\tau - \tau') C_u(\tau') d\tau', \quad (50)$$

$$K(\tau - \tau') = \frac{x_A^2}{2\pi} \int_0^\infty dx \frac{\tilde{\Gamma}_0(x)}{x^2} \left[1 + \bar{\xi}^\perp(\mathbf{r}_A, x) + \left(\frac{x}{x_A} \right)^2 \bar{\xi}^\parallel(\mathbf{r}_A, x) \right] \times \frac{e^{-i(x - \tilde{x}_A)(\tau - \tau')} - 1}{i(x - \tilde{x}_A)} \quad (51)$$

with the \mathbf{r}_A -dependent transverse and longitudinal local photonic DOS functions $\bar{\xi}^\perp(\mathbf{r}_A, x)$ and $\bar{\xi}^\parallel(\mathbf{r}_A, x)$ given explicitly by Eqs. (42) and (43), respectively,

$$\tilde{\Gamma}_0(x) = \frac{\hbar}{2\gamma_0} \Gamma_0(x) = \frac{4d_z^2}{3\hbar c^3} \left(\frac{2\gamma_0}{\hbar} \right)^2 x^3 \quad (52)$$

being the dimensionless vacuum spontaneous decay rate (37), and

$$\tilde{x}_A = x_A \left[1 - \frac{1}{\pi} \int_0^\infty dx \frac{\tilde{\Gamma}_0(x)}{x^2} \bar{\xi}^\perp(\mathbf{r}_A, x) \right] \quad (53)$$

representing the dimensionless renormalized transition frequency (28) where a divergent contribution to the vacuum Lamb shift has been omitted since the true (renormalized) vacuum Lamb shift may be considered as included in the atomic transition frequency x_A [12, 13].

Eq. (50) is a well-known Volterra integral equation of the second kind, which in our case describes spontaneous decay dynamics of an excited two-level atomic system interacting with the vacuum electromagnetic field modified by the presence of a CN. All the CN parameters that are relevant for the spontaneous decay are contained in the local photonic DOS functions in the kernel (51). The latter ones are, in view of Eqs. (34), (40) and (41), determined by the imaginary classical Green tensor of the CN modified electromagnetic field.

4.1 Qualitative Analysis

Let us first analyze qualitatively the time dynamics of the upper state population probability $C_u(\tau)$ in terms of two different approximations admitting analytical solutions of the evolution problem (50), (51). They are the Markovian approximation and the single-resonance approximation of the local photonic DOS in the vicinity of the CN.

4.1.1 Markovian Approximation

Suppose the atom is faraway from the CN. Obviously, the local photonic DOS functions $\bar{\xi}^\perp(\mathbf{r}_A, x)$ and $\bar{\xi}^\parallel(\mathbf{r}_A, x)$ are then small in their values and the atom-field coupling matrix elements (32) and (33) are mainly contributed by the free space term which comes from the unity in ξ^\perp [see Eqs. (34), (38)–(41)]. In this particular case, the Markovian approximation is applicable for sure. The latter one is known to be an excellent approximation for describing the radiative decay of an excited atom in free space where the atom-field coupling strength is weak enough for atomic motion memory effects to be insignificant, so that they may be neglected [58]. The time-dependent factor in the kernel (51) may then be replaced by its long-time approximation (see, e.g., [49])

$$\frac{e^{-i(x-\tilde{x}_A)(\tau-\tau')} - 1}{i(x-\tilde{x}_A)} \rightarrow -\pi\delta(x-\tilde{x}_A) + i\frac{\mathcal{P}}{x-\tilde{x}_A}, \quad (54)$$

(\mathcal{P} denotes a principal value) where $\tilde{x}_A \approx x_A$ according to Eq. (53) with small enough $\bar{\xi}^\perp(\mathbf{r}_A, x)$. In so doing, the kernel (51) becomes

$$K(\tau - \tau') = -\frac{1}{2}\tilde{\Gamma}(x_A) + i\Delta(x_A) \quad (55)$$

and the evolution equation (50) yields

$$C_u(\tau) = \exp\left[-\frac{1}{2}\tilde{\Gamma}(x_A) + i\Delta(x_A)\right]\tau \quad (56)$$

– the exponential decay dynamics of the upper atomic level shifted by

$$\Delta(x_A) = \frac{\mathcal{P}}{2\pi} \int_0^\infty dx \frac{\tilde{\Gamma}_0(x)}{x-x_A} \left[\left(\frac{x_A}{x}\right)^2 \bar{\xi}^\perp(\mathbf{r}_A, x) + \bar{\xi}^\parallel(\mathbf{r}_A, x) \right] \quad (57)$$

[here, a divergent contribution to the vacuum Lamb shift has been omitted for the same reason as that in Eq. (53)] with the rate

$$\tilde{\Gamma}(x_A) = \tilde{\Gamma}_0(x_A) \left[1 + \bar{\xi}^\perp(\mathbf{r}_A, x_A) + \bar{\xi}^\parallel(\mathbf{r}_A, x_A) \right] \quad (58)$$

accounting for the presence of the nanotube.

4.1.2 Single-Resonance Approximation of the Local Photonic DOS

Another approximation that admits an analytical solution of the evolution problem (50), (51) is the single-resonance approximation of the local photonic DOS. Suppose the functions $\bar{\xi}^\perp(\mathbf{r}_A, x)$ and $\bar{\xi}^\parallel(\mathbf{r}_A, x)$ have sharp peaks at $x = x_r$ [the fact that they have the same positions of extrema is obvious from Eqs. (42) and (43); see also the footnote on page 28]. For all x in the vicinity of x_r , their shape may then be roughly approximated by the Lorentzian functions with the same half-width-at-half-maximum δx_r of the form

$$\bar{\xi}^{\perp(\parallel)}(\mathbf{r}_A, x) \approx \bar{\xi}^{\perp(\parallel)}(\mathbf{r}_A, x_r) \frac{\delta x_r^2}{(x - x_r)^2 + \delta x_r^2}. \quad (59)$$

The integrand in the kernel (51) is seen to be basically contributed by $x \sim \tilde{x}_A$, thus making it possible to approximate the factor in the square brackets as follows

$$1 + \bar{\xi}^\perp(\mathbf{r}_A, x) + \left(\frac{x}{x_A} \right)^2 \bar{\xi}^\parallel(\mathbf{r}_A, x) \approx 1 + \bar{\xi}^\perp(\mathbf{r}_A, x) + \left(\frac{\tilde{x}_A}{x_A} \right)^2 \bar{\xi}^\parallel(\mathbf{r}_A, x)$$

with \tilde{x}_A given in an explicit form by Eq. (53). Keeping this and the Lorentzian approximation (59) in mind, one calculates the kernel (51) analytically to linear approximation in δx_r to obtain

$$K(\tau - \tau') \approx \tilde{\Gamma}(x_r) \frac{\delta x_r}{2} \frac{\exp[-i(x_r - i\delta x_r - \tilde{x}_A)(\tau - \tau')] - 1}{i(x_r - i\delta x_r - \tilde{x}_A)}, \quad \tau > \tau' \quad (60)$$

with $\tilde{\Gamma}(x_r)$ given by Eq. (58). Substituting this into Eq. (50) and making the differentiation of both sides of the resulting equation over time, followed by the change of the integration order and one more time differentiation, one straightforwardly arrives at a second order ordinary homogeneous differential equation of the form

$$\ddot{C}_u(\tau) + i(x_r - i\delta x_r - \tilde{x}_A)\dot{C}_u(\tau) + (X/2)^2 C_u(\tau) = 0, \quad (61)$$

where

$$X = \sqrt{2\delta x_r \tilde{\Gamma}(x_r)}, \quad (62)$$

with the solution given for $\tilde{x}_A \approx x_r$ by

$$C_u(\tau) \approx \frac{1}{2} \left(1 + \frac{\delta x_r}{\sqrt{\delta x_r^2 - X^2}} \right) \exp \left[- \left(\delta x_r - \sqrt{\delta x_r^2 - X^2} \right) \frac{\tau}{2} \right] \\ + \frac{1}{2} \left(1 - \frac{\delta x_r}{\sqrt{\delta x_r^2 - X^2}} \right) \exp \left[- \left(\delta x_r + \sqrt{\delta x_r^2 - X^2} \right) \frac{\tau}{2} \right]. \quad (63)$$

This solution is approximately valid for those atomic transition frequencies \tilde{x}_A which are located in the vicinity of the photonic DOS resonances whatever the atom-field coupling strength is. In particular, if $(X/\delta x_r)^2 \ll 1$, Eq. (63) yields the exponential decay of the upper atomic state population probability $|C_u(\tau)|^2$ with the rate $\tilde{\Gamma}(x_r)$ in full agreement with Eq. (56) obtained within the Markovian approximation for weak atom-field coupling. In the opposite case, when $(X/\delta x_r)^2 \gg 1$, one has

$$|C_u(\tau)|^2 \approx e^{-\delta x_r \tau} \cos^2 \left(\frac{X\tau}{2} \right), \quad (64)$$

and the decay of the upper atomic state population probability proceeds via damped Rabi oscillations with the dimensionless Rabi frequency X given by Eq. (62). This is the principal signature of strong atom-field coupling which is beyond the Markovian approximation. Expressing $\tilde{\Gamma}(x_r)$ in Eq. (62) in terms of the local photonic DOS functions by means of Eqs. (58), (40), (41) and approximating for atomic systems with Coulomb interaction $\tilde{\Gamma}_0(x) \approx 137^{-3}x$ [49], one may conveniently rewrite the strong atom-field coupling condition in the form

$$2x_r \frac{\xi^\perp(x_r) + \xi^\parallel(x_r)}{137^3 \delta x_r} \gg 1, \quad (65)$$

from which it follows that the strong coupling regime is fostered by high and narrow resonances in the local photonic DOS.

4.2 Numerical Results and Discussion

To get beyond the Markovian and single-resonance approximations, we have solved Eqs. (50) and (51) numerically. The *exact* time evolution of the upper state population probability $|C_u(\tau)|^2$ was obtained for the atom placed [in a way that Eq. (45) was always satisfied] in the center and near the wall inside, and at different distances outside achiral CNs of different radii. The local photonic DOS functions were computed according to Eqs. (40)–(43). The CN surface axial conductivity σ_{zz} appearing in Eqs. (42), (43) was calculated in the relaxation-time approximation with the relaxation time 3×10^{-12} s; the spatial dispersion of σ_{zz} was neglected [39]. The vacuum contribution to the kernel (51) (that coming from the unity in the square brackets) was taken into account within the Markovian approximation (54) with the divergent vacuum Lamb shift omitted as the true (renormalized) vacuum Lamb shift may be

considered as included in the 'bare' atomic transition frequency x_A [12, 13]. The Markovian approximation is known to be an excellent approximation for describing atom-radiation interaction processes in free space [58]. The vacuum spontaneous decay rate was approximated by the expression $\tilde{\Gamma}_0(x) \approx 137^{-3}x$ valid for atomic systems with Coulomb interaction [49].

Figure 3 (a) presents $\xi^\perp(x)$ for the atom in the center of the (5,5), (10,10) and (23,0) CNs. It is seen to decrease with increasing the CN radius, representing the decrease of the atom-field coupling strength as the atom moves away from the CN surface. To calculate $|C_u(\tau)|^2$ in this particular case, we have fixed $x_A=0.45$ (indicated by the vertical dashed line), firstly, because this transition is located within the visible light range $0.305 < x < 0.574$, secondly, because this is the approximate peak position of $\xi^\perp(x)$ for all the three CNs. The functions $|C_u(\tau)|^2$ calculated are shown in Figure 2 (b) in comparison with those obtained in the Markovian approximation yielding the exponential decay. The actual spontaneous decay dynamics is clearly seen to be non-exponential. For the small radius (5,5) CN, Rabi oscillations are observed, indicating a *strong* atom-field coupling regime related to *strong* non-Markovian memory effects. Eq. (65) is satisfied in this case. With increasing the CN radius, as the value of $\xi^\perp(0.45)$ decreases, Eq. (65) ceases to be valid and the decay dynamics approaches the exponential one with the decay rate enhanced by several orders of magnitude compared with that in free space. Note that, though the distance from the atom to the CN surface is larger for the (23,0) CN than for the (10,10) CN, the deviation of the actual decay dynamics from the exponential one is larger for the (23,0) CN. This is an obvious consequence of the influence of a small neighboring peak in the (23,0) CN photonic density of states [Figure 3 (a)].

In Ref. [5], formation of Cs-encapsulating single-wall CNs was reported. In a particular case of the (10,10) CN, the stable Cs atom/ion position was observed to be at distance of 3 Å from the wall. We have simulated the spontaneous decay dynamics for a number of typical atomic transition frequencies for this case. Figure 4 (a) shows the local photonic DOS and the five specific transition frequencies x_A (dashed lines) for which the functions $|C_u(t)|^2$ presented in Figure 4 (b) were calculated. Rabi oscillations are clearly seen to occur in the vicinity of the highest peak ($x_A \approx 0.22$) of the photonic density of states. Important is that they persist for large enough detuning values $x_A \approx 0.21 \div 0.25$. For $x_A = 0.30$, the density of photonic states has a dip, and the decay dynamics exhibits no Rabi oscillations, being strongly non-exponential nevertheless. For $x_A = 0.45$, the intensity of the peak of the photonic density of states is not large enough and the peak is too broad, so that the strong atom-field coupling condition (65) is not satisfied and the decay dynamics is close to the exponential one.

Figure 5 (a) shows the local photonic DOS for the atom outside the (9,0) CN at the different distances from its surface. The vertical dashed lines indicate the atomic transitions for which the functions $|C_u(\tau)|^2$ in Figures 5 (b), (c), and (d) were calculated. The transitions $x_A=0.33$ and 0.58 are the positions of sharp peaks

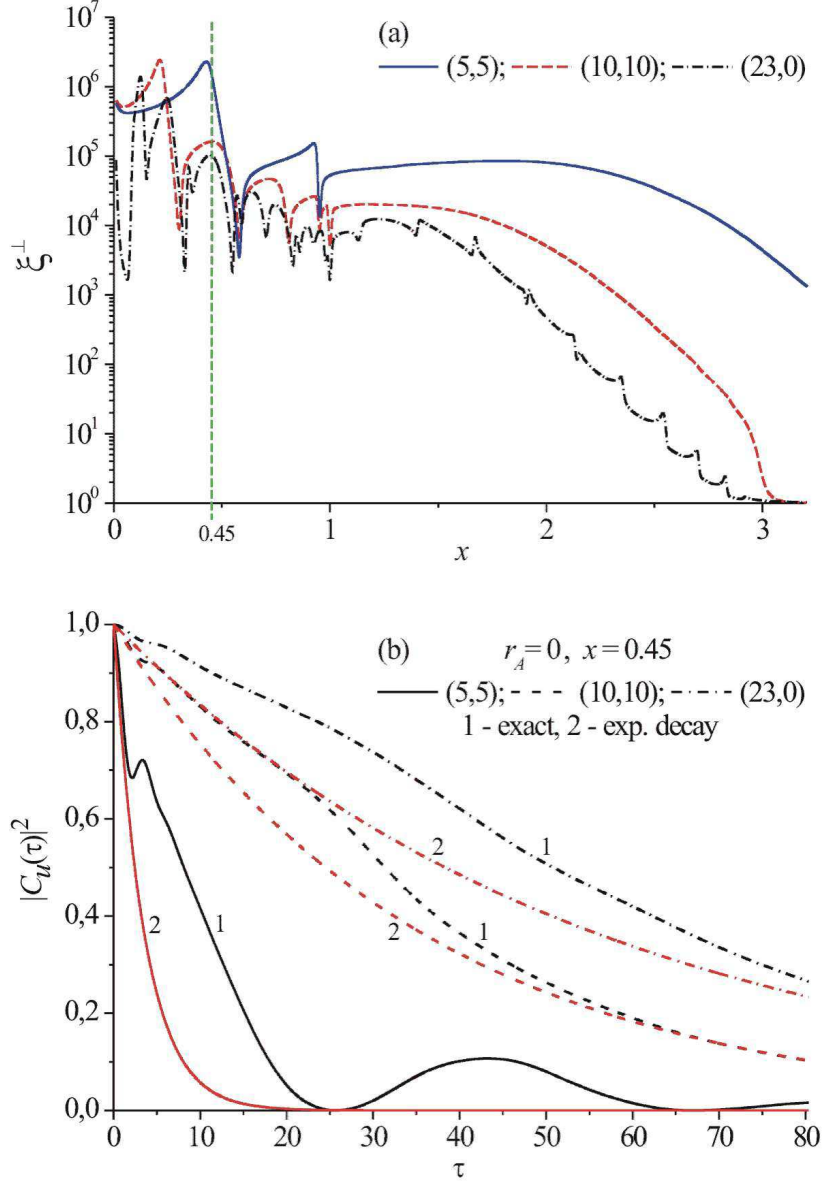


Figure 3: Transverse local photonic DOS's (a) and upper-level spontaneous decay dynamics (b) for the atom in the center of different CNs. The ('bare') atomic transition frequency is indicated by the dashed line in Fig. 3 (a).

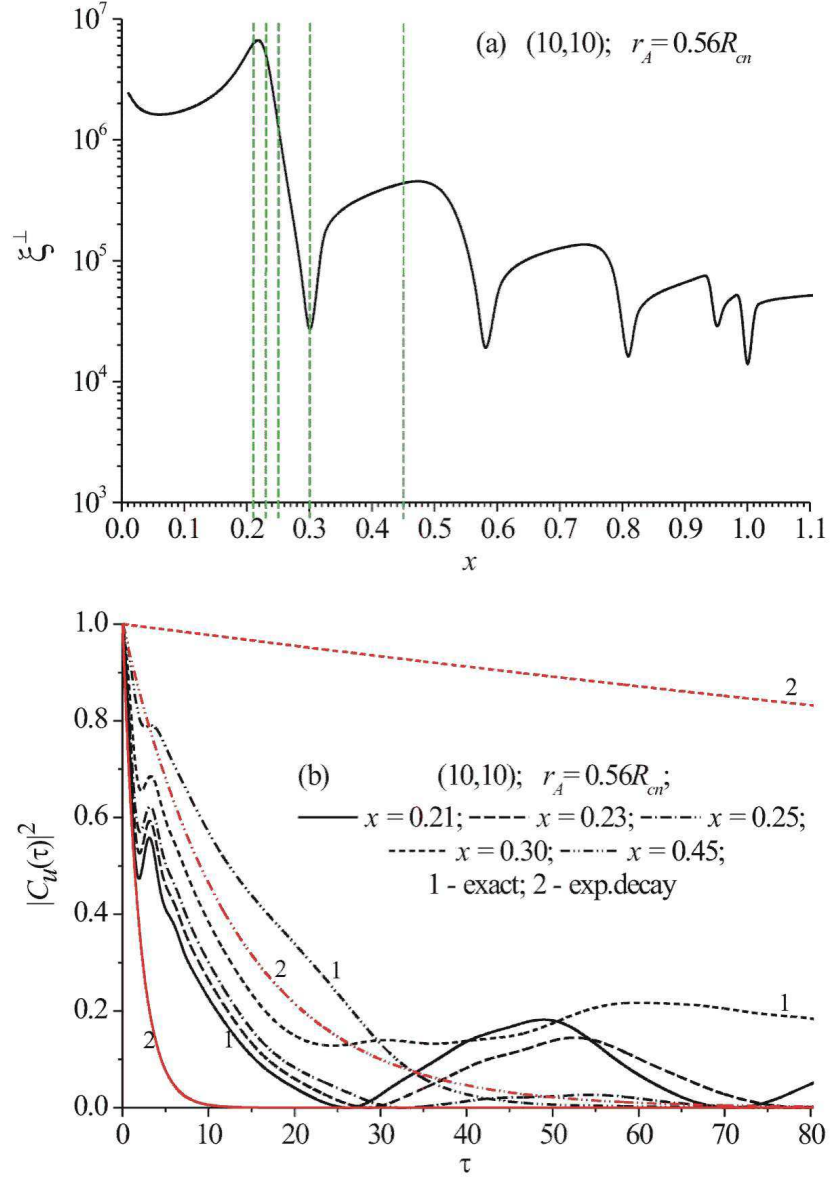


Figure 4: (a) Fragment of the transverse local photonic DOS for the atom inside the (10,10) CN at distance of 3 Å from the wall (the situation observed experimentally for Cs in Ref. [5]). (b) Upper-level spontaneous decay dynamics for different ('bare') atomic transition frequencies [indicated by the dashed lines in Fig. 4 (a)] in this particular case.

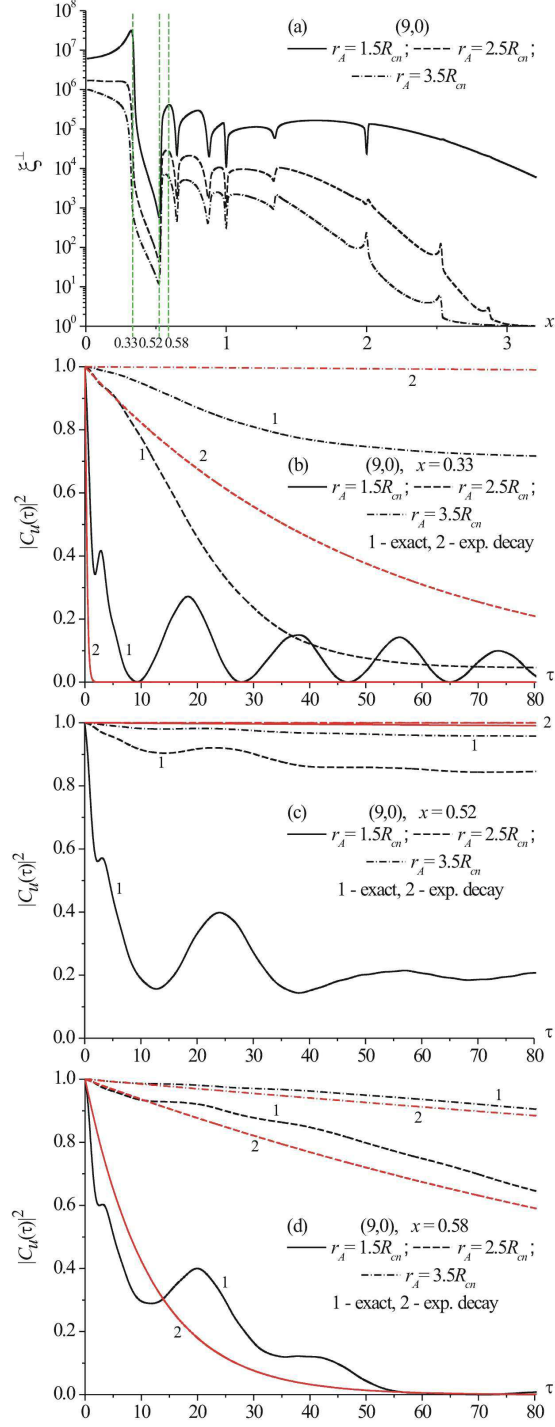


Figure 5: (a) Transverse local photonic DOS's for the atom located at different distances outside the (9,0) CN. (b, c, d) Upper-level spontaneous decay dynamics for the three ('bare') atomic transition frequencies [indicated by the dashed lines in Fig. 5 (a)] at different atom-nanotube-surface distances.

(at least for the shortest atom-surface distance), while $x_A = 0.52$ is the position of a dip of the function $\xi^\perp(x)$. Very clear underdamped Rabi oscillations are seen for the shortest atom-surface distance at $x_A = 0.33$ [Figure 4 (b)], indicating strong atom-field coupling with strong non-Markovity. For $x_A = 0.58$ [Figure 5 (d)], the value of $\xi^\perp(0.58)$ is not large enough for strong atom-field coupling to occur, so that Eq. (65) is not fulfilled. As a consequence, the decay dynamics, being strongly non-exponential in general, exhibits no clear Rabi oscillations. For $x_A = 0.52$ [Figure 5 (c)], though $\xi^\perp(0.52)$ is comparatively small, the spontaneous decay dynamics is still non-exponential, approaching the exponential one only when the atom is far enough from the CN surface.

The reason for non-exponential spontaneous decay dynamics in all the cases considered is similar to that taking place in photonic crystals [16]. When the atom is close enough to the CN surface, an absolute value of the relative density of photonic states is large and its frequency variation in the neighborhood of a specific atomic transition frequency essentially influences the time behavior of the kernel (51) of the evolution equation (50). Physically, this means that the correlation time of the electromagnetic vacuum is not negligible on the time scale of the evolution of the atomic system, so that atomic motion memory effects are important and the Markovian approximation in the kernel (51) is inapplicable. The drastic increase of the local photonic DOS near a CN can be interpreted as being due to the electromagnetic vacuum renormalization: the relative density of photonic states near the CN effectively increases since, along with ordinary free photons, there appear surface photonic states coupled with CN electronic quasiparticle excitations. These latter ones are responsible for the nonradiative atomic decay (photon emission by the atom with subsequent CN quasiparticle excitation) [26]. Obviously, such a decay does not respond sensitively to the microscopic radiation-field structure in a close vicinity of the CN surface. This, along with Eq. (45), justifies rather small atom-surface distances we have considered within the macroscopic Green-tensor approach.

5 van der Waals Energy of a Ground-State Atom near a Carbon Nanotube

When the atom is in the ground state, its vdW energy near the nanotube is given by the \mathbf{r}_A -dependent contribution to the ground-state eigenvalue of the total Hamiltonian (23)-(26). Important, however, is that the unperturbed atomic subsystem is now described by the Hamiltonian (25) with the renormalized transition frequency (28). Eqs. (53) and (44) represent the latter one in terms of the transverse \mathbf{r}_A -dependent photonic DOS $\bar{\xi}^\perp(\mathbf{r}_A, x)$. They indicate that the transition frequency $\tilde{\omega}_A$ decreases with increasing $\bar{\xi}^\perp$, i. e. when the atom approaches the CN surface [see Fig. 5 (a) as an example], thereby bringing the unperturbed atomic levels together, or even making them degenerated if $\bar{\xi}^\perp$ is large enough [see the schematic

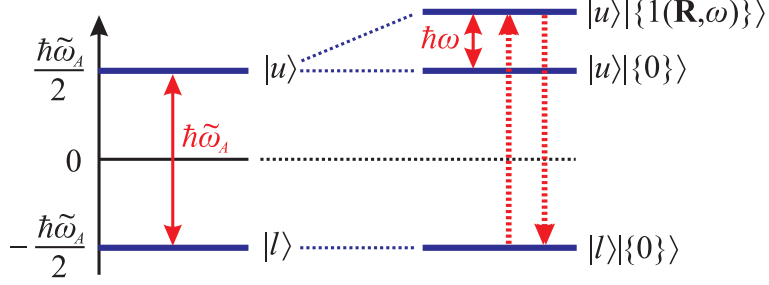


Figure 6: Schematic of the energy levels in the problem of the ground-state atom vdW interaction with the CN. On the left are the unperturbed atomic levels given by the Hamiltonian (25), on the right are the levels of the coupled "atom-nanotube" system given by the total Hamiltonian (23)–(26). The relevant virtual transition of the system is shown by the vertical dashed arrows. See Eqs. (53) and (44) for $\tilde{\omega}_A$.

of the energy levels of the problem in Fig. 6 and a typical example of the (9,0) CN in Fig. 7]. If one uses the standard perturbation theory, this would yield the divergence of high-order corrections to the vdW energy at small atom-CN-surface distances because of the small energy denominators in the corresponding power-series expansions. To account for a possible degeneracy of the unperturbed atomic levels in a correct way, one has to use the perturbation theory for degenerated atomic levels (see, e.g., [49]). In so doing, one has to take the upper state degeneracy into account of the whole system with respect to \mathbf{R} as well as its possible degeneracy with respect to ω when $\omega \sim \tilde{\omega}_A \sim 0$ as is seen in Fig. 6. Thus, the ground-state wave function of the whole system should be represented as a coherent mixture of the lower and upper states of the form

$$|\psi\rangle = C_l |l\rangle|\{0\}\rangle + \int_0^\infty d\omega \int d\mathbf{R} C_u(\mathbf{R}, \omega) |u\rangle|\{1(\mathbf{R}, \omega)\}\rangle, \quad (66)$$

where C_l and $C_u(\mathbf{R}, \omega)$ are unknown mixing coefficients of the lower and upper states of the *whole* system.

The total energy E of the ground state is now given by the solution of a secular equation obtained by applying the Hamiltonian (23)–(26) to the wave function (66). This yields the integral equation

$$E = -\frac{\hbar\tilde{\omega}_A}{2} - \int_0^\infty d\omega \int d\mathbf{R} \frac{|g^{(-)}(\mathbf{r}_A, \mathbf{R}, \omega)|^2}{\hbar\omega + \frac{\hbar\tilde{\omega}_A}{2} - E}, \quad (67)$$

which the ground-state-atom vdW energy $E_{vw}(\mathbf{r}_A)$ is determined from by means of an obvious relationship

$$E = -\frac{\hbar\omega_A}{2} + E_{vw}(\mathbf{r}_A) \quad (68)$$

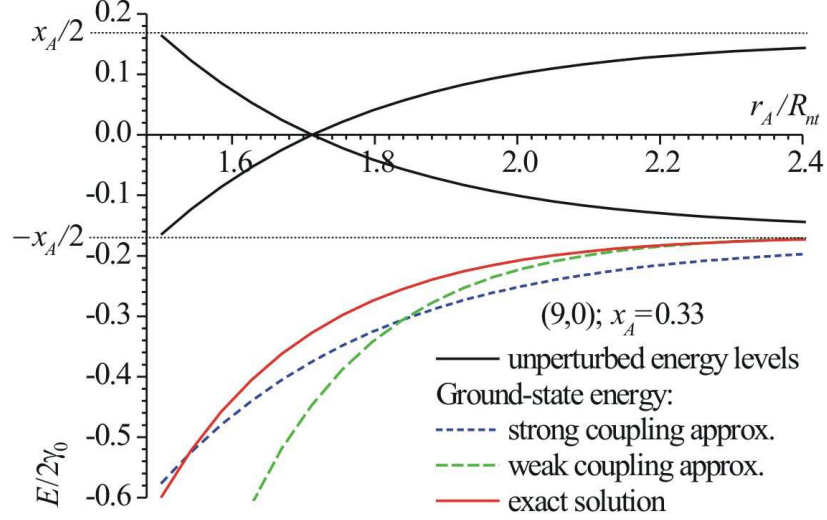


Figure 7: Dimensionless unperturbed energy levels [given by the Hamiltonian (24) and (25)] and total ground-state energy [given by Eqs. (68)–(70), (42) and (43)] as functions of the atomic position for the two-level atom outside the (9,0) CN. See Eq. (44) for x_A .

with the first term representing the 'bare' (non-interacting) two-level atom in the ground-state. This, upon recalling Eqs. (33), (40), (41) and (44) and introducing the dimensionless vdW energy

$$\varepsilon_{vw}(\mathbf{r}_A) = \frac{E_{vw}(\mathbf{r}_A)}{2\gamma_0}, \quad (69)$$

reduces to the integral equation of the form

$$\begin{aligned} \varepsilon_{vw}(\mathbf{r}_A) = & \frac{x_A}{2\pi} \int_0^\infty dx \frac{\tilde{\Gamma}_0(x)}{x^2} \bar{\xi}^\perp(\mathbf{r}_A, x) \\ & - \frac{x_A^2}{2\pi} \int_0^\infty dx \frac{\tilde{\Gamma}_0(x)}{x^2} \frac{\bar{\xi}^\perp(\mathbf{r}_A, x) + \left(\frac{x}{x_A}\right)^2 \bar{\xi}^\parallel(\mathbf{r}_A, x)}{x + x_A \left[1 - \frac{1}{2\pi} \int_0^\infty dx \frac{\tilde{\Gamma}_0(x)}{x^2} \bar{\xi}^\perp(\mathbf{r}_A, x) \right] - \varepsilon_{vw}(\mathbf{r}_A)}, \end{aligned} \quad (70)$$

representing the dimensionless ground-state-atom vdW energy in terms of the transverse and longitudinal \mathbf{r}_A -dependent (local) photonic DOS functions $\bar{\xi}^\perp(\mathbf{r}_A, x)$ and $\bar{\xi}^\parallel(\mathbf{r}_A, x)$, which are given in an explicit form by Eqs. (42) and (43), respectively.

5.1 Qualitative Analysis

Eqs. (68)–(70) along with Eqs. (42) and (43) describe the ground-state-atom vdW energy near an infinitely long single-wall carbon nanotube in terms of the local (distance-dependent) photonic DOS. Eq. (70) is universal in the sense that it covers both strong and weak atom-field coupling regimes defined as those violating and non-violating, respectively, the applicability domain of the conventional stationary perturbation theory.²

5.1.1 Weak Coupling Regime

If, when the atom is faraway from the CN, the local photonic DOS $\bar{\xi}^\perp(\mathbf{r}_A, x)$ is such small that

$$\frac{1}{2\pi} \int_0^\infty dx \frac{\tilde{\Gamma}_0(x)}{x^2} \bar{\xi}^\perp(\mathbf{r}_A, x) \ll 1 \quad (71)$$

and

$$|\varepsilon_{vw}(\mathbf{r}_A)| \ll x_A, \quad (72)$$

then Eq. (70) yields a well-known perturbation theory result (see, e.g., [29, 30]) of the form

$$\begin{aligned} \varepsilon_{vw}(\mathbf{r}_A) \approx & \frac{x_A}{2\pi} \int_0^\infty dx \frac{\tilde{\Gamma}_0(x)}{x^2} \bar{\xi}^\perp(\mathbf{r}_A, x) \\ & - \frac{x_A^2}{2\pi} \int_0^\infty dx \frac{\tilde{\Gamma}_0(x)}{x^2} \frac{\bar{\xi}^\perp(\mathbf{r}_A, x) + \left(\frac{x}{x_A}\right)^2 \bar{\xi}^\parallel(\mathbf{r}_A, x)}{x + x_A}, \end{aligned} \quad (73)$$

where the first term comes from the unperturbed Hamiltonian (24), (25) and the second one is the second order correction due to the perturbation (26). This can be equivalently rewritten in the form

$$\varepsilon_{vw}(\mathbf{r}_A) \approx \frac{x_A}{2\pi} \int_0^\infty dx \frac{\tilde{\Gamma}_0(x)}{x(x + x_A)} \left[\bar{\xi}^\perp(\mathbf{r}_A, x) - \frac{x}{x_A} \bar{\xi}^\parallel(\mathbf{r}_A, x) \right], \quad (74)$$

from which, in view of Eqs. (42), (43) and basic properties of the modified cylindric Bessel functions (see, e.g. [56, 59]), one can immediately come to an interesting conclusion. Namely, if the atom is fixed outside (inside) the CN in a way that the weak atom-field coupling regime is realized, i.e. far enough from the CN surface, then the modulus of the atom-nanotube vdW energy increases (decreases) with the CN radius. The conclusion is physically clear as the effective atom-nanotube interaction

²One should make a clear difference between this definition and that where the strong (weak) atom-field coupling regime is defined as that violating (non-violating) the applicability domain of the Markovian approximation [16]. Our definition here is based on the Born approximation associated with the strength of the coupling between the atom and the photonic reservoir, whereas the Markovian approximation is related to memory effects of the photonic reservoir.

area is larger (smaller) for larger-radius nanotubes when the atom is outside (inside) the CN. Important, however, is that this obvious conclusion is, strictly speaking, only valid in the weak atom-field coupling regime for the outside atomic position, while for the inside atomic position it represents a general effect of the effective interaction area reduction with lowering the CN surface curvature.

In the large CN radius limit, Eq. (74) along with Eqs. (42) and (43) can be shown to reproduce a well-known Casimir-Polder result [60] for an atom near an infinitely conducting plane (see Appendix C).

5.1.2 Strong Coupling Regime

When the atom is close enough to the CN surface, the local photonic DOS $\bar{\xi}^\perp(\mathbf{r}_A, x)$ is large, so that one might expect the condition

$$\frac{1}{2\pi} \int_0^\infty dx \frac{\tilde{\Gamma}_0(x)}{x^2} \bar{\xi}^\perp(\mathbf{r}_A, x) \sim 1 \quad (75)$$

to hold true. Under this condition, Eq. (70) reduces to an integral equation of the form

$$\begin{aligned} \varepsilon_{vw}(\mathbf{r}_A) \approx & \frac{x_A}{2\pi} \int_0^\infty dx \frac{\tilde{\Gamma}_0(x)}{x^2} \bar{\xi}^\perp(\mathbf{r}_A, x) \\ & - \frac{x_A^2}{2\pi} \int_0^\infty dx \frac{\tilde{\Gamma}_0(x)}{x^2} \frac{\bar{\xi}^\perp(\mathbf{r}_A, x) + \left(\frac{x}{x_A}\right)^2 \bar{\xi}^\parallel(\mathbf{r}_A, x)}{x - \varepsilon_{vw}(\mathbf{r}_A)} \end{aligned} \quad (76)$$

valid in the strong atom-field coupling regime.

Eq. (75) corresponds to the *inverted* unperturbed atomic levels described by the Hamiltonian (25) with $\tilde{\omega}_A$ given by Eqs. (53) and (44) (see Fig. 7 as an example). The levels are degenerated when the left-hand side of Eq. (75) is exactly 0.5. A noteworthy point is that if one used the weak coupling approximation of Eq. (70) for the atom close to the CN surface where Eq. (71) is not satisfied and Eq. (75) holds true instead, then the result would be divergent at the lower limit of integration. To avoid this fact, one has to use either the strong coupling approximation (76) or the exact equation (70) to calculate the vdW energy of the atom close to the nanotube surface.

5.2 Numerical Results and Discussion

Using Eqs. (68)–(70) along with (42) and (43), we have simulated the total ground state energy of the whole system "two-level atom + CN-modified vacuum electromagnetic field" and the vdW energy of the two-level atom nearby metallic and semi-conducting carbon nanotubes of different radii. The dimensionless free-space spontaneous decay rate in Eq. (70) was approximated by the expression $\tilde{\Gamma}_0(x) \approx 137^{-3}x$ valid for atomic systems with Coulomb interaction [49].

Figure 7 shows the dimensionless ground state energy level of the whole system [given by the corresponding eigenvalue of the total Hamiltonian (23)–(26) and represented by Eqs. (68)–(70)] and two dimensionless energy levels of the unperturbed Hamiltonian (24), (25) as functions of the atomic position outside the (9,0) CN. As the atom approaches the CN surface, its unperturbed levels come together, then get degenerated and even inverted at a very small atom-surface distance. In so doing, the weak coupling approximation for the ground state energy [given by Eqs. (68), (69), (74) and (42), (43)] diverges near the surface, whereas the strong coupling approximation [Eqs. (68), (69), (76) and (42), (43)] yields a finite result. The exact solution reproduces the weak coupling approximation at large and the strong coupling approximation at short atom-surface distances, respectively. Close to the nanotube surface, the exact solution is seen to be a little bit lower than that given by the strong coupling approximation (76). This is because the condition (75) turns into the inequality in this region with the left-hand side larger than unity that is not taken into account by the equation (76).

The degeneracy of the unperturbed atomic levels is the consequence of the transverse local photonic DOS increase [see Eq. (53)] as the atom approaches the CN surface. A typical example is shown in Fig. 5 (a) for the atom outside the (9,0) CN. The transverse DOS function is seen to increase with decreasing the atom-CN-surface distance, representing the atom-field coupling strength enhancement with surface photonic modes of the nanotube as the atom approaches the nanotube surface. The longitudinal local photonic DOS behaves in a similar way as is seen in Fig. 8 (a).³ The vertical dashed lines in Fig. 8 (a) indicate the 'bare' atomic transition frequencies x_A for which the vdW energies shown in Fig. 8 (b) were calculated. Some of them are the positions of peaks, the others are the positions of dips of the local photonic DOS. They are typical for some rear-earth ions such as Europium, or for heavy hydrogen-like atoms such as Caesium (supposed to be non-ionized near the CN). For example [18], for a well-known two-level dipole transition ${}^7F_2 \leftrightarrow {}^5D_0$ of Europium at $\lambda = 615$ nm one has $x_A \approx 0.37$, whereas for Caesium one obtains from its first ionization potential [61] the estimate $x_A \approx 3.89 \text{ eV} \times 3/4 \times (2\gamma_0)^{-1} \approx 0.5$ (the factor $3/4$ comes from the Lyman series of Hydrogen), or less for highly excited Rydberg states.

Figure 8 (b) shows the vdW energies of the atom outside the (9,0) CN for three different 'bare' atomic transition frequencies indicated by vertical dashed lines in Fig. 8 (a). Here, exact numerical solutions of Eqs. (68)–(70), (42), (43) are compared with those obtained within the weak coupling approximation (74), (42), (43)

³For the small atom-CN-surface distances illustrated here, the electromagnetic field retardation effects play no role and the transverse and longitudinal DOS functions are actually exactly the same. Indeed, taking the limit $c \rightarrow \infty$ allows one to set $v = h$ in Eqs. (114) and (115) in Appendix B, thereby making the transverse and longitudinal DOS functions identical in the non-retarded limit. Both of these functions are proportional to c^3 , but this large factor is cancelled out by the c^3 factor in the denominator of the dimensionless vacuum spontaneous decay rate (52) that multiplies the photonic DOS functions in all the expressions.

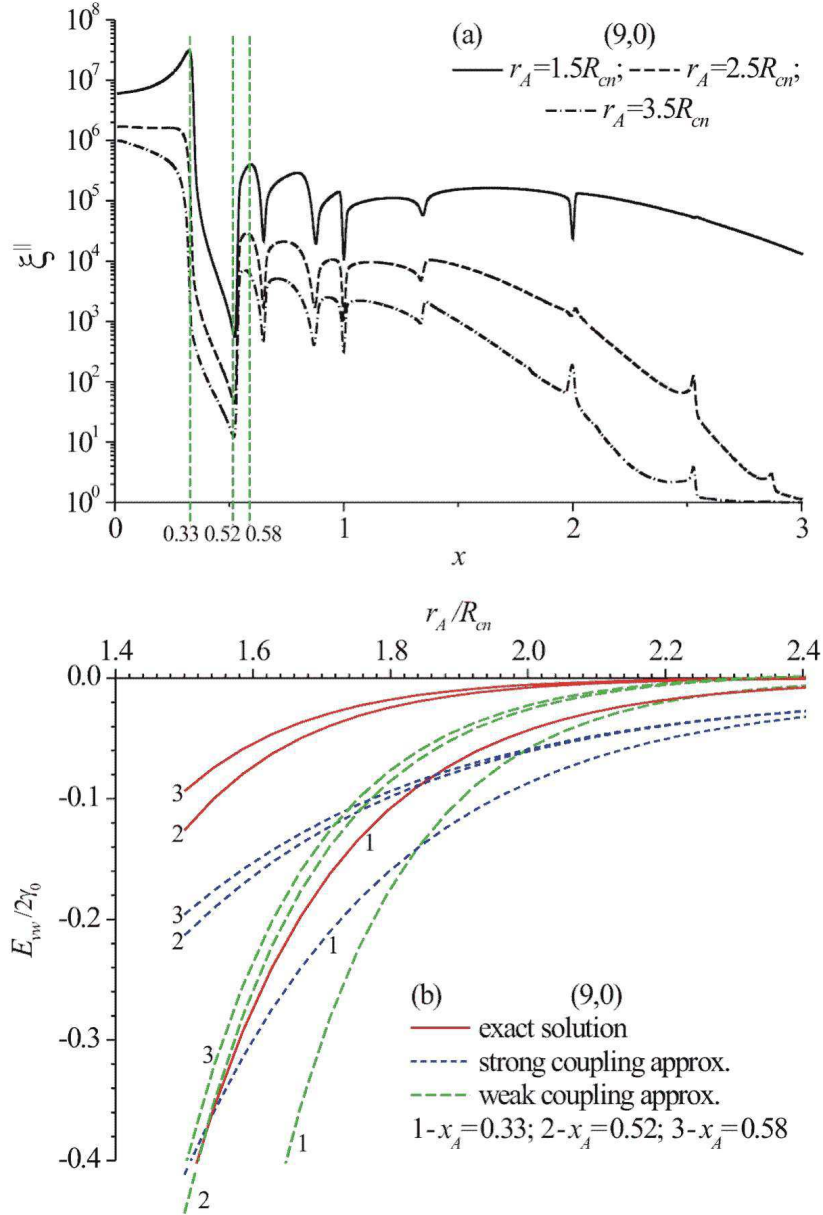


Figure 8: Longitudinal local photonic DOS's (a) and ground-state vdW energies (b) as functions of the atomic position for the two-level atom outside the (9,0) CN. The ('bare') atomic transition frequencies are indicated by dashed lines in Fig. 8 (a).

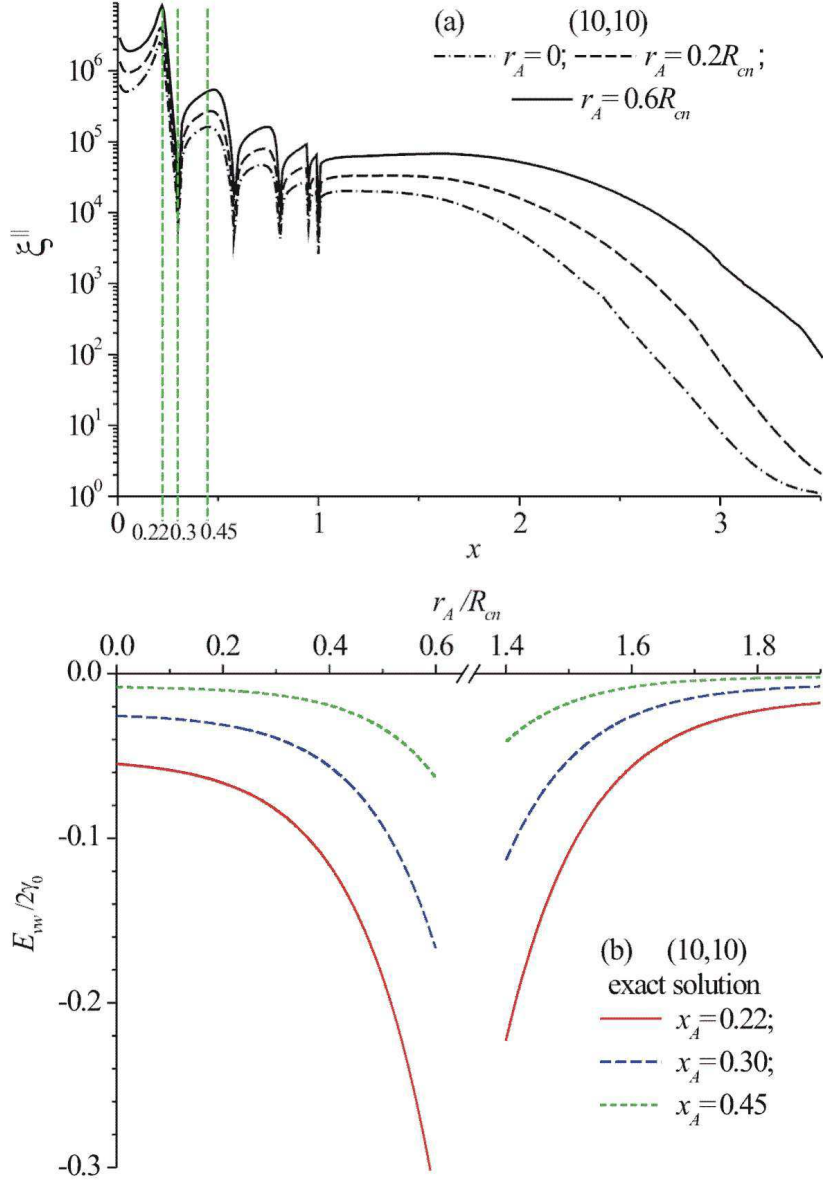


Figure 9: Longitudinal local photonic DOS's (a) and ground-state vdW energies (b) as functions of the atomic position for the two-level atom nearby the (10,10) CN. The ('bare') atomic transition frequencies are indicated by dashed lines in Fig. 9 (a).

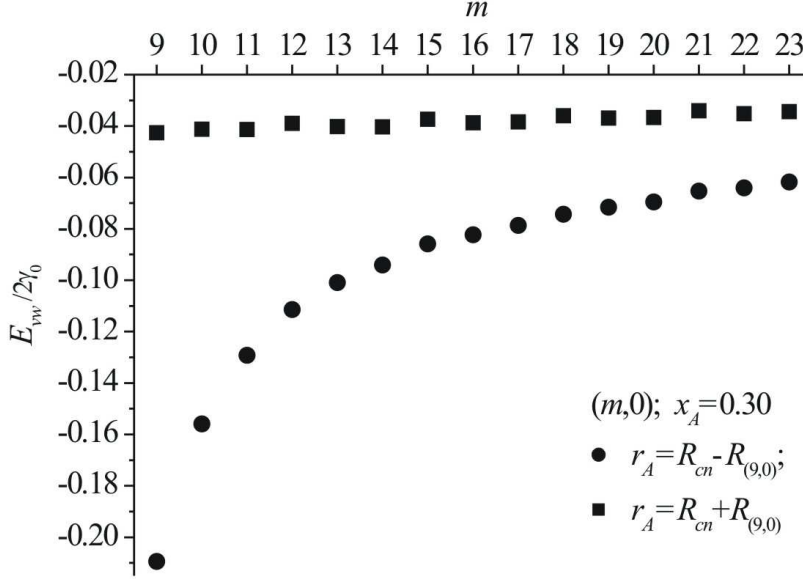


Figure 10: Ground-state van der Waals energy of the two-level atom positioned at a fixed atom-surface distance [equal to the radius of the (9,0) CN] inside and outside "zigzag" $(m, 0)$ CNs of different radii, as a function of the nanotube index m .

and within the strong coupling approximation (76), (42), (43). At small atom-CN-surface distances, the exact solutions are seen to be fairly well reproduced by those obtained in the strong coupling approximation, clearly indicating the strong atom-field coupling regime in a close vicinity of the nanotube surface. The deviation from the strong coupling approximation increases with transition frequency x_A , that is easily explicable since the degeneracy condition (75) of the unperturbed atomic levels is more difficult to reach for larger inter-level separations. As the atom moves away from the CN surface, the exact solutions deviate from the strong coupling solutions and approach those given by the weak coupling approximation, indicating the reduction of the atom-field coupling strength with raising the atom-surface distance. The weak-coupling solutions are seen to be divergent close to the nanotube surface as it should be because of the degeneracy of the unperturbed atomic levels in this region.

Figure 9 (a) shows the longitudinal local photonic DOS's for the atom inside the (10,10) CN at three representative distances from the nanotube wall. As the atom approaches the wall, the longitudinal DOS function increases in a similar way as that Fig. 8 (a) for the outside atomic position. The vertical dashed lines indicate the 'bare'

atomic transition frequencies for which the atomic vdW energies in Fig. 9 (b) were calculated. Figure 9 (b) represents the exact solutions of Eq. (70) for atom inside and outside the (10,10) CN. When the atom is inside, the vdW energies are seen to be in general lower than those for the atom outside the CN. This may be attributed to the fact that, due to the nanotube curvature, the effective interaction area between the atom and the CN surface is larger when the atom is inside rather than when it is outside the CN. This, in turn, indicates that encapsulation of doped atoms into the nanotube is energetically more favorable than their outside adsorption by the nanotube surface – the effect observed experimentally in Ref. [5].

Comparing Fig. 8 (b) with Fig. 9 (b) for the outside atomic position, one can see that, if the atom-CN-surface distance is so large that the weak-coupling approximation is good, then for the same distance and approximately the same atomic transition frequency $x_A \approx 0.3$ the vdW energy near the (10,10) nanotube ($R_{cn} = 6.78 \text{ \AA}$) is lower than that near the (9,0) nanotube ($R_{cn} = 3.52 \text{ \AA}$). This is in agreement with the qualitative predictions formulated above in analyzing the weak coupling regime. In the present case, the effective atom-CN-surface interaction area is larger for the atom outside the larger-radius (10,10) nanotube, thereby explaining the effect. Obviously, one should expect an opposite effect for the inside atomic position. Experimentally, the heat of absorption of Krypton, to take an example, has been shown to be larger for graphite (0.17 eV/atom) than for multiwall nanotubes (0.12 eV/atom) [62], in agreement with our theoretical predictions.

A similar tendency is demonstrated in Fig 10. Here, the vdW energies calculated from Eqs. (68)–(70), (42), (43) are represented for the atom positioned at a fixed distance from the nanotube wall [chosen to be equal to the radius of the (9,0) CN] inside and outside the "zigzag" ($m, 0$) CNs of increasing radius $R_{cn} = m(a\sqrt{3}/2\pi)$. When the atom is inside, the energy absolute value goes down with R_{cn} , representing a general tendency of the effective interaction area reduction with lowering the CN surface curvature. When the atom is outside, the effect would be the opposite one if the atom were weakly coupled to the field, thus indicating that the atom-field coupling regime is not actually weak for the distance chosen. In general, the inside and outside vdW energies approach each other with R_{cn} as it should be since the two atomic positions become equivalent in the plane limit where $R_{cn} \rightarrow \infty$. Interesting is also the fact that the vdW energies of the atom outside the metallic nanotubes (m is divisible by 3) are on average a little bit smaller than those for the atom outside semiconducting ones. This is certainly the property related to the difference in conductivities of metallic and semiconducting "zigzag" nanotubes. The property can be understood qualitatively as follows. In view of the absence of the longitudinal depolarization [40], the CN dielectric tensor zz -component $\epsilon_{zz}(\mathbf{R}, \omega)$ is related to the longitudinal polarizability $\alpha_{zz}(\omega)$ of the CN per unit length via the equation

$$\epsilon_{zz}(\mathbf{R}, \omega) = 1 + 4\pi\rho_T l_T \alpha_{zz}(\omega)$$

with l_T being the length of the tubule. This, via the Drude relationship (4), yields

$$\sigma_{zz}(\mathbf{R}, \omega) = -i\omega \frac{\alpha_{zz}(\omega)}{2\pi R_{cn}}$$

from which it immediately follows that larger real conductivities inherent to metallic CNs lead to larger imaginary polarizabilities corresponding to stronger optical absorption by metallic CNs compared with semiconducting ones. It is then obvious that virtual long-wavelength photon exchange responsible for the long-range London-type dispersion vdW interaction is suppressed for the atom outside the metallic CNs due to their stronger absorption compared with the semiconducting CNs.

6 Conclusion

We have developed the quantum theory of near-field electrodynamical properties of carbon nanotubes and investigated spontaneous decay dynamics of excited states and van der Waals attraction of the ground state of an atomic system (an atom or a molecule) close to a single-wall nanotube surface. In describing the atom-field interaction, we followed the electromagnetic field quantization scheme developed for dispersing and absorbing media in Refs. [12, 13]. This quantization formalism was adapted by us for a particular case of an atom near an infinitely long single-wall CN. We derived the simplified secondly quantized Hamiltonian representing the "atom-nanotube" coupled system in terms of only two standard approximations. They are the electric dipole approximation and the atomic two-level approximation. The (commonly used [25]) rotating wave approximation was not applied and the diamagnetic term of the atom-field interaction was not neglected. Starting with this general Hamiltonian, we have obtained an evolution equation for the population probability of the upper state and a vdW energy equation of the lower (ground) state of the two-level atomic system coupled with the CN modified vacuum electromagnetic field. The equations are represented in terms of the local photonic DOS and are valid for both strong and weak atom-field coupling regime.

By solving the evolution equation of the upper state of the system numerically, we have demonstrated a strictly non-exponential spontaneous decay dynamics in the case where the atom is close enough to the CN surface. In certain cases, namely when the atom is close enough to the nanotube surface and the atomic transition frequency is in the vicinity of the resonance of the local photonic DOS, the system exhibits vacuum-field Rabi oscillations – a principal signature of strong atom-vacuum-field coupling. This is the result of strong non-Markovian memory effects arising from the rapid frequency variation of the photonic DOS near the nanotube. The non-exponential decay dynamics gives place to the exponential one if the atom moves away from the CN surface. Thus, the atom-vacuum-field coupling strength and the character of the spontaneous decay dynamics, respectively, may be controlled by

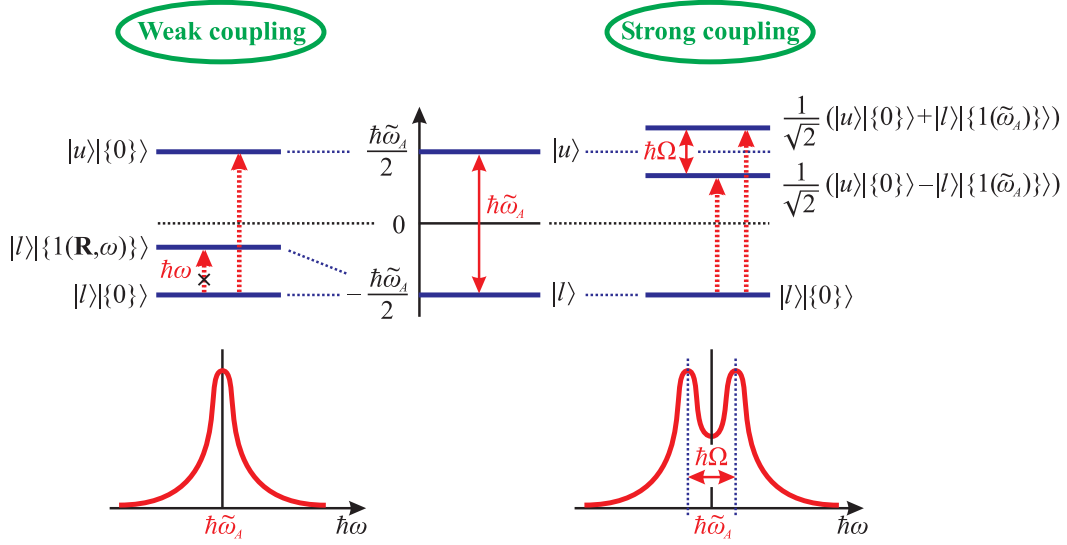


Figure 11: Schematic of the energy levels and the absorption line-shapes expected in the optical absorbance experiment with atomically doped CNs. In the center are the unperturbed atomic levels given by the Hamiltonian (25). On the left and on the right are the levels of the coupled "atom-nanotube" system in the weak and strong atom-vacuum-field coupling regime, respectively. The system is excited by an external optical radiation. The allowed and forbidden (crossed) optical transitions are shown by vertical dashed arrows. See Eqs. (53), (62) and (44) for $\tilde{\omega}_A$ and Ω .

changing the distance between the atom and CN surface by means of a proper preparation of atomically doped CN systems.

We would like to emphasize a general character of the conclusion above and its applied and fundamental significance. We have shown that similar to semiconductor microcavities [19, 21, 46] and photonic band-gap materials [16, 23], carbon nanotubes may qualitatively change the character of the atom-electromagnetic-field interaction, yielding strong atom-field coupling. The study of such phenomena was started awhile ago in atomic physics [63] and still attracts a lot of interest in connection with various quantum optics and nanophotonics applications [11, 24, 64, 65] as well as quantum computation and quantum information processing [9, 66, 67, 68]. The fact that the carbon nanotube may control atom-electromagnetic-field coupling opens routes for new challenging applications of atomically doped CN systems as various sources of coherent light emitted by dopant atoms.

Strong atom-vacuum-field coupling we predict will yield an additional structure in optical absorbance/reflectance spectra (see, e.g., [43, 44]) of atomically doped CNs in the vicinity of the energy of an atomic transition. The illustration is shown in Fig. 11. Weak non-Markovity of the atom-vacuum-field interactions (that yield-

ing non-exponential spontaneous decay dynamics with no Rabi oscillations) will cause an asymmetry of an optical spectral line-shape (not shown in Fig. 11) similar to that taking place for the exciton optical absorption line-shape in quantum dots [69]. Strong non-Markovity of the atom-vacuum-field interactions (yielding non-exponential spontaneous decay dynamics with fast Rabi oscillations) originates from strong atom-vacuum-field coupling with the upper state of the system splitted into two "dressed" states (see Fig. 11, on the right). This will yield a two-component structure of optical absorbance/reflectance spectra similar to that observed for excitonic and intersubband electronic transitions in semiconductor quantum microcavities [45, 46].

The atomic state strongly coupled to the surface vacuum photonic modes of the nanotube is nothing but a 'quasi-1D cavity polariton' similar by its physical nature to quasi-2D excitonic [45], intersubband electronic [46] and quasi-0D excitonic [19, 21] polaritons in semiconductor quantum microcavities as well as to quasi-0D excitonic polaritons in photonic crystal nanocavities [23] recently observed experimentally. Obviously, the stability of quasi-1D atomic polaritons in CNs is basically determined by the atom-nanotube van der Waals interaction. This interaction, however, originates from *strong* atom-field coupling and, therefore, cannot be correctly described in terms of vacuum-QED-based (weak-coupling) vdW interaction models as well as in terms of those based upon the linear response theory. We have developed a simple quantum mechanical approach to the ground-state vdW energy calculation of a two-level atomic system near a CN. The approach is based upon the perturbation theory for degenerated atomic levels, thus accounting for both weak and strong atom-field coupling and thereby covering the vdW interactions of the ground-state quasi-1D atomic polaritons in CNs. Within the framework of this approach, the vdW energy is described by the integral equation represented in terms of the local photonic DOS. By solving this equation numerically, we have demonstrated the inapplicability of weak-coupling-based vdW interaction models in a close vicinity of the nanotube surface where the local photonic DOS effectively increases, giving rise to an atom-field coupling enhancement followed by the degeneracy of the unperturbed atomic levels due to the diamagnetic interaction term.

The fundamental conclusion above is supplemented by those important for various applications of atomically doped CNs in modern nanotechnology. In particular, we have studied CN surface curvature effects on the atom-nanotube vdW interactions and have shown that an inside encapsulation of doped atoms into the nanotube is energetically more favorable than their outside adsorption by the nanotube surface, in agreement with the experimental observations reported in Ref. [5]. Moreover, if the atom is fixed outside the CN in a way that the weak atom-field coupling regime is realized, i.e. far enough from the CN surface, then the modulus of the atom-nanotube vdW energy increases with the CN radius because the effective atom-nanotube interaction area is larger for larger-radius nanotubes in this case. For inside atomic position, the modulus of the atom-nanotube vdW energy decreases

with the CN radius, representing a general effect of the effective interaction area reduction with lowering the CN surface curvature.

Finally, we here only dealt with the simplest manifestations of the strong coupling regime in the atom-electromagnetic-field interactions near carbon nanotubes. Similar manifestations of strong atom-field coupling may occur in many other atom-electromagnetic-field interaction processes in the presence of CNs, such as, e.g., atomic states entanglement [70], interatomic dipole-dipole interactions [71, 72], cascade spontaneous transitions in three-level atomic systems [73], etc. A further intriguing extension of the present work could also be the study of the vdW interactions of excited atomic states where, even in the weak atom-field-coupling regime and in the simplest case of an atom near a planar semi-infinite medium, very interesting peculiarities (e.g., oscillatory behavior) were recently shown to exist [30].

Acknowledgements

The authors would like to thank G. Abstreiter, I.D. Feranchuk, J. Finley, G.Ya. Slepian and D.-G. Welsch for fruitful discussions.

A Two-level approximation

In this Appendix, we rewrite the Hamiltonian (18)–(22) in terms of a two-level atomic model [25]. Within the framework of this model, the spectrum of the atomic Hamiltonian (20) is approximated by the two eigenstates, upper $|u\rangle$ and lower $|l\rangle$, with the energies $\hbar\omega_u$ and $\hbar\omega_l$, respectively. One has then

$$\hat{H}_A \approx \hbar\omega_u |u\rangle\langle u| + \hbar\omega_l |l\rangle\langle l| \quad (77)$$

with a completeness relation

$$|u\rangle\langle u| + |l\rangle\langle l| = \hat{I}. \quad (78)$$

Subtracting a constant term $(\hbar/2)(\omega_u + \omega_l)\hat{I}$ from the Hamiltonian (77) and thereby placing the energy zero in the middle between the two energy levels, one arrives at the 'bare' two-level atomic Hamiltonian of the form

$$\hat{H}_A = \frac{\hbar\omega_A}{2} \hat{\sigma}_z \quad (79)$$

with $\hat{\sigma}_z = |u\rangle\langle u| - |l\rangle\langle l|$ and $\omega_A = \omega_u - \omega_l$ being the 'bare' atomic transition frequency.

In terms of such a two-level scheme, the atomic dipole moment operator $\hat{\mathbf{d}}$ has the matrix elements $\langle u|\hat{\mathbf{d}}|l\rangle = \langle l|\hat{\mathbf{d}}|u\rangle = \mathbf{d}$ and $\langle u|\hat{\mathbf{d}}|u\rangle = \langle l|\hat{\mathbf{d}}|l\rangle = 0$. Keeping this and the completeness relation (78) in mind, the interaction Hamiltonians (21) and (22) can be rewritten as follows.

For the interaction (21), using Eqs. (8) and (9) and a well-known quantum mechanical operator equality

$$(\hat{\mathbf{p}}_i)_\alpha = m_i \frac{d}{dt} (\hat{\mathbf{r}}_i)_\alpha = \frac{m_i}{i\hbar} [(\hat{\mathbf{r}}_i)_\alpha, \hat{H}_A], \quad (80)$$

where the Latin and Greek indexes enumerate particles in the atom and vector components, respectively, and \hat{H}_A is given by Eq. (79), one has

$$\begin{aligned} \hat{H}_{AF}^{(1)} &= (\hat{\sigma} - \hat{\sigma}^\dagger) \mathbf{d} \cdot \left[\int_0^\infty d\omega \frac{\omega_A}{\omega} \underline{\hat{\mathbf{E}}}^\perp(\mathbf{r}_A, \omega) - \text{h.c.} \right] \\ &\quad - (\hat{\sigma} + \hat{\sigma}^\dagger) \mathbf{d} \cdot \left[\int_0^\infty d\omega \underline{\hat{\mathbf{E}}}^\parallel(\mathbf{r}_A, \omega) + \text{h.c.} \right], \end{aligned} \quad (81)$$

with $\hat{\sigma} = |l\rangle\langle u|$ and $\hat{\sigma}^\dagger = |u\rangle\langle l|$. Using further Eqs. (10), (16) and (5) and assuming the longitudinal (along the CN axis) atomic dipole orientation due to the dominant axial polarizability of the nanotube [40, 41, 42, 43, 44], one arrives at the secondly quantized interaction Hamiltonian (26) with the interaction matrix elements (29) and (30).

For the interaction (22), one may proceed as follows

$$\begin{aligned} \hat{H}_{AF}^{(2)} &= \sum_{i,j} \sum_{\alpha,\beta} \frac{q_i q_j}{2m_i c^2} \delta_{ij} \delta_{\alpha\beta} \hat{A}_\alpha(\mathbf{r}_A) \hat{A}_\beta(\mathbf{r}_A) \\ &= \frac{i}{2\hbar c^2} \sum_{i,\alpha,\beta} \frac{q_i}{m_i} [(\hat{\mathbf{p}}_i)_\alpha, \hat{d}_\beta] \hat{A}_\alpha(\mathbf{r}_A) \hat{A}_\beta(\mathbf{r}_A), \end{aligned} \quad (82)$$

where the product of the two Kronecker-symbols in the first line is represented in terms of the 'coordinate-momentum' commutator as

$$\delta_{ij} \delta_{\alpha\beta} = \frac{i}{\hbar} [(\hat{\mathbf{p}}_i)_\alpha, (\hat{\mathbf{r}}_j)_\beta].$$

Using Eq. (80) for the momentum operator components and the completeness relation (78), one arrives at

$$\hat{H}_{AF}^{(2)} = -\frac{\omega_A}{\hbar c^2} \hat{\sigma}_z \left[\mathbf{d} \cdot \hat{\mathbf{A}}(\mathbf{r}_A) \right]^2 \quad (83)$$

which, upon substituting Eq. (8) for the vector potential operator, becomes

$$\begin{aligned} & -\frac{\hat{\sigma}_z}{\hbar \omega_A} \sum_{\alpha,\beta} d_\alpha d_\beta \left\{ \int_0^\infty d\omega \frac{\omega_A}{i\omega} \int_0^\infty d\omega' \frac{\omega_A}{i\omega'} \underline{\hat{\mathbf{E}}}^\perp_\alpha(\mathbf{r}_A, \omega) \underline{\hat{\mathbf{E}}}^\perp_\beta(\mathbf{r}_A, \omega') \right. \\ & \quad \left. - \int_0^\infty d\omega \frac{\omega_A}{i\omega} \int_0^\infty d\omega' \frac{\omega_A}{i\omega'} \underline{\hat{\mathbf{E}}}^\perp_\alpha(\mathbf{r}_A, \omega) \left[\underline{\hat{\mathbf{E}}}^\perp_\beta(\mathbf{r}_A, \omega') \right]^\dagger + \text{h.c.} \right\}. \end{aligned}$$

The four items here can, in view of Eqs. (10), (16) and (5), be classified as follows. The first item and its hermitian conjugate describe the processes with simultaneous annihilation and creation of *two* photons (two-photon transitions). They may be safely neglected if the field intensity is low enough that, we believe, is the case for the vacuum electromagnetic field we deal with in considering the vdW interactions. Furthermore, keeping them in the Hamiltonian $\hat{H}_{AF}^{(2)}$ is meaningless as the Hamiltonian $\hat{H}_{AF}^{(1)}$ is nothing but a dipole approximation which, by its definition, neglects two-photon transitions. The second item and its hermitian conjugate are combined together by using bosonic commutation relations (2) to give in terms of the bosonic field operators and the transverse dipole interaction matrix element (30) the expression

$$-\frac{\hat{\sigma}_z}{\hbar\omega_A} \int_0^\infty d\omega \int d\mathbf{R} |g^\perp(\mathbf{r}_A, \mathbf{R}, \omega)|^2 \\ - \frac{2\hat{\sigma}_z}{\hbar\omega_A} \int_0^\infty d\omega d\omega' \int d\mathbf{R} d\mathbf{R}' \left[g^\perp(\mathbf{r}_A, \mathbf{R}, \omega) \right]^* g^\perp(\mathbf{r}_A, \mathbf{R}', \omega') f^\dagger(\mathbf{R}, \omega) f(\mathbf{R}', \omega'),$$

where the second term is nothing but a two-photon correction to the dipole interaction (26), that can be easily seen by noting that $\hat{\sigma}_z = \hat{\sigma}^\dagger \hat{\sigma} - \hat{\sigma} \hat{\sigma}^\dagger$. This correction must be neglected for the reasons just discussed, so that finally one arrives at

$$\hat{H}_{AF}^{(2)} \approx -\frac{\hat{\sigma}_z}{\hbar\omega_A} \int_0^\infty d\omega \int d\mathbf{R} |g^\perp(\mathbf{r}_A, \mathbf{R}, \omega)|^2. \quad (84)$$

Eq. (84) can now be combined with the 'bare' atomic Hamiltonian (79) to yield the 'effective' unperturbed atomic Hamiltonian (25) with the renormalized atomic transition frequency given by Eq. (28).

Thus, we have proved that the Hamiltonian (18)–(22), being approximated in terms of the two-level atomic model, is represented by the Hamiltonian (23)–(26).

B Green tensor and local photonic DOS

(a) Green tensor of a single-wall carbon nanotube

We start with Eq. (17) for the Green tensor of the electromagnetic subsystem. This equation is a direct consequence of the equation

$$\sum_{\alpha=r,\varphi,z} (\nabla \times \nabla \times - k^2)_{z\alpha} \hat{\underline{E}}_\alpha(\mathbf{r}, \omega) = i \frac{4\pi}{c} k \hat{\underline{I}}_z(\mathbf{r}, \omega) \quad (85)$$

obtained by substituting the magnetic field operator from Eq. (13) into Eq. (14). On the other hand, under the condition of the Coulomb gauge (see, e.g., [51]), one has

$$\hat{\underline{E}}(\mathbf{r}, \omega) = \hat{\underline{E}}^\perp(\mathbf{r}, \omega) + \hat{\underline{E}}^\parallel(\mathbf{r}, \omega) \quad (86)$$

with [compare with Eqs. (8) and (9)]

$$\hat{\underline{\mathbf{E}}}^\perp(\mathbf{r}, \omega) = ik\hat{\underline{\mathbf{A}}}(\mathbf{r}, \omega), \quad (87)$$

where

$$\nabla \cdot \hat{\underline{\mathbf{A}}}(\mathbf{r}, \omega) = 0, \quad (88)$$

and

$$\hat{\underline{\mathbf{E}}}^\parallel(\mathbf{r}, \omega) = -\nabla\varphi(\mathbf{r}, \omega). \quad (89)$$

From Eqs. (85)–(89), in view of Eq. (10) and (16), one obtains the following equation for the Green tensor components

$$\sum_{\alpha=r,\varphi,z} (\nabla \times \nabla \times - k^2)_{z\alpha} \left[{}^\perp G_{\alpha z}(\mathbf{r}, \mathbf{R}, \omega) + {}^\parallel G_{\alpha z}(\mathbf{r}, \mathbf{R}, \omega) \right] = \delta(\mathbf{r} - \mathbf{R}) \quad (90)$$

with additional constraints

$$\sum_{\alpha=r,\varphi,z} \nabla_\alpha {}^\perp G_{\alpha z}(\mathbf{r}, \mathbf{R}, \omega) = 0 \quad (91)$$

and

$$\sum_{\beta,\gamma=r,\varphi,z} \epsilon_{\alpha\beta\gamma} \nabla_\beta {}^\parallel G_{\gamma z}(\mathbf{r}, \mathbf{R}, \omega) = 0, \quad (92)$$

where $\epsilon_{\alpha\beta\gamma}$ is the totally antisymmetric unit tensor of rank 3. Keeping Eqs. (91) and (92) in mind, Eq. (90) is rewritten to give two independent equations for the transverse and longitudinal Green tensors of the form

$$(\Delta + k^2) {}^\perp G_{zz}(\mathbf{r}, \mathbf{R}, \omega) = -\delta_{zz}^\perp(\mathbf{r} - \mathbf{R}), \quad (93)$$

$$k^2 {}^\parallel G_{zz}(\mathbf{r}, \mathbf{R}, \omega) = -\delta_{zz}^\parallel(\mathbf{r} - \mathbf{R}) \quad (94)$$

with the transverse and longitudinal δ -functions given by Eqs. (11) and (12), respectively, and ${}^{\perp(\parallel)} G_{zz}(\mathbf{r}, \mathbf{R}, \omega)$ defined by Eq. (31).

Electromagnetic properties of the "atom–nanotube" coupled system are, according to Eqs. (32)–(34), determined by the Green functions ${}^\perp G_{zz}^\perp(\mathbf{r}_A, \mathbf{r}_A, \omega)$ and ${}^\parallel G_{zz}^\parallel(\mathbf{r}_A, \mathbf{r}_A, \omega)$. To derive them, we start with ${}^\perp G_{zz}(\mathbf{r}, \mathbf{r}_A, \omega)$ for which we use the differential representation

$${}^\perp G_{zz}(\mathbf{r}, \mathbf{r}_A, \omega) = \left(\frac{1}{k^2} \nabla_z \nabla_z + 1 \right) g(\mathbf{r}, \mathbf{r}_A, \omega) \quad (95)$$

equivalent to Eq. (31). Here, $g(\mathbf{r}, \mathbf{r}_A, \omega)$ is the Green function of the scalar Helmholtz equation which satisfies the radiation condition at infinity and boundary conditions on the CN surface. Indeed, substituting Eq. (95) into Eq. (93) and using Eq. (91), one straightforwardly obtains

$$(\Delta + k^2) g(\mathbf{r}, \mathbf{r}_A, \omega) = -\delta_{zz}^\perp(\mathbf{r} - \mathbf{r}_A) \quad (96)$$

– the scalar Helmholtz equation with a transverse δ -source. For the longitudinal Green function $\parallel G_{zz}(\mathbf{r}, \mathbf{r}_A, \omega)$, one analogously has

$$\parallel G_{zz}(\mathbf{r}, \mathbf{r}_A, \omega) = -\frac{1}{k^2} \nabla_z \nabla_z g(\mathbf{r}, \mathbf{r}_A, \omega), \quad (97)$$

which upon substituting into Eq. (94) yields

$$\nabla_z \nabla_z g(\mathbf{r}, \mathbf{r}_A, \omega) = \delta_{zz}^{\parallel}(\mathbf{r} - \mathbf{r}_A). \quad (98)$$

Eq. (96) has a known solution

$$g_0(\mathbf{r}, \mathbf{r}_A, \omega) = \frac{1}{4\pi} \frac{e^{ik|\mathbf{r}-\mathbf{r}_A|}}{|\mathbf{r} - \mathbf{r}_A|} \quad (99)$$

satisfying the radiation condition at infinity (see, e.g., [49]). In our case, however, the functions

$$^{\perp}G_{\alpha z}(\mathbf{r}, \mathbf{r}_A, \omega) = \left(\frac{1}{k^2} \nabla_{\alpha} \nabla_z + \delta_{\alpha z} \right) g(\mathbf{r}, \mathbf{r}_A, \omega) \quad (100)$$

and $g(\mathbf{r}, \mathbf{r}_A, \omega)$, respectively, are imposed one more set of boundary conditions. They are the boundary conditions on the surface of the CN. Using simple relations

$$\underline{E}_{\alpha}(\mathbf{r}, \omega) = ik^{\perp} G_{\alpha z}(\mathbf{r}, \mathbf{r}_A, \omega) \quad (101)$$

$$\underline{H}_{\alpha}(\mathbf{r}, \omega) = -\frac{i}{k} \sum_{\beta, \gamma=r, \varphi, z} \epsilon_{\alpha\beta\gamma} \nabla_{\beta} E_{\gamma}(\mathbf{r}, \omega), \quad (102)$$

valid at $\mathbf{r} \neq \mathbf{r}_A$ for a classical electromagnetic field under the Coulomb-gauge condition [51], they can be derived from the classical electromagnetic field boundary conditions of the form

$$\underline{E}_{\varphi}|_{r=R_{cn}+0} - \underline{E}_{\varphi}|_{r=R_{cn}-0} = 0, \quad (103)$$

$$\underline{E}_z|_{r=R_{cn}+0} - \underline{E}_z|_{r=R_{cn}-0} = 0, \quad (104)$$

$$\underline{H}_{\varphi}|_{r=R_{cn}+0} - \underline{H}_{\varphi}|_{r=R_{cn}-0} = \frac{4\pi}{c} \sigma_{zz}(R_{cn}, \omega) \underline{E}_z|_{r=R_{cn}}, \quad (105)$$

$$\underline{H}_z|_{r=R_{cn}+0} - \underline{H}_z|_{r=R_{cn}-0} = 0 \quad (106)$$

(spatial dispersion neglected) obtained in Ref. [39].

Let $r_A > R_{cn}$ (the atom is outside the CN) to be specific. Then, the function $g(\mathbf{r}, \mathbf{r}_A, \omega)$, being the complete solution of Eq. (96), is represented as a sum of

a particular solution of the inhomogeneous equation and a general solution of the homogeneous equation in the form

$$g(\mathbf{r}, \mathbf{r}_A, \omega) = \begin{cases} g_0(\mathbf{r}, \mathbf{r}_A, \omega) + g^{(+)}(\mathbf{r}, \omega), & r > R_{cn} \\ g^{(-)}(\mathbf{r}, \omega), & r < R_{cn} \end{cases} \quad (107)$$

where $g_0(\mathbf{r}, \mathbf{r}_A, \omega)$ is the point radiative atomic source function defined by Eq. (99) and $g^{(\pm)}(\mathbf{r}, \omega)$ are unknown nonsingular functions satisfying the homogeneous Helmholtz equation and the radiation conditions at infinity. We seek them using integral decompositions over the modified cylindric Bessel functions I_p and K_p as follows [51]

$$g^{(\pm)}(\mathbf{r}, \omega) = \sum_{p=-\infty}^{\infty} e^{ip\varphi} \int_C \left\{ \begin{array}{c} A_p(h) K_p(vr) \\ B_p(h) I_p(vr) \end{array} \right\} e^{ihz} dh \quad (108)$$

and

$$g_0(\mathbf{r}, \mathbf{r}_A, \omega) = \frac{1}{(2\pi)^2} \sum_{p=-\infty}^{\infty} e^{ip\varphi} \int_C I_p(vr) K_p(vr_A) e^{ihz} dh, \quad r_A \geq r, \quad (109)$$

where $A_p(h)$ and $B_p(h)$ are unknown functions to be found from the boundary conditions (103)–(106) in view of Eqs. (100), (101) and (102), $v = v(h, \omega) = \sqrt{h^2 - k^2}$. The integration contour C runs along the real axis of the complex plane and envelopes the branch points $\pm k$ from below and from above, respectively. The coordinate system has been fixed as is shown in Fig. 1.

The boundary conditions (103)–(106) with Eqs. (100), (101) and (102) taken into account yield the following two independent equations for the scalar Green function (107)

$$g_0(\mathbf{r}, \mathbf{r}_A, \omega)|_{r=R_{cn}} + g^{(+)}(\mathbf{r}, \omega)|_{r=R_{cn}} = g^{(-)}(\mathbf{r}, \omega)|_{r=R_{cn}},$$

$$\begin{aligned} & \frac{\partial g^{(+)}(\mathbf{r}, \omega)}{\partial r} \Big|_{r=R_{cn}} - \frac{\partial g^{(-)}(\mathbf{r}, \omega)}{\partial r} \Big|_{r=R_{cn}} \\ & + \beta(\omega) \left(\frac{\partial^2}{\partial z^2} + k^2 \right) g^{(-)}(\mathbf{r}, \omega) \Big|_{r=R_{cn}} = - \frac{\partial g_0(\mathbf{r}, \mathbf{r}_A, \omega)}{\partial r} \Big|_{r=R_{cn}}, \end{aligned}$$

where $\beta(\omega) = 4\pi i \sigma_{zz}(R_{cn}, \omega)/\omega$. Substituting the integral decompositions (108) and (109) into these equations, one obtains the set of two simultaneous algebraic equations for the functions $A_p(h)$ and $B_p(h)$. The function $A_p(h)$ we need (we only need the Green function in the region where the atom is located) is found by solving this set with the use of basic properties of cylindric Bessel functions (see, e.g., [56, 59]). In so doing, one has

$$A_p(h) = - \frac{R_{cn} \beta(\omega) v^2 I_p^2(v R_{cn}) K_p(v r_A)}{(2\pi)^2 [1 + \beta(\omega) v^2 R_{cn} I_p(v R_{cn}) K_p(v R_{cn})]}.$$

These $A_p(h)$, being substituted into Eq. (108), yield the function $g^{(+)}(\mathbf{r}, \omega)$ sought. The latter one, in view of Eq. (107), results in the scalar electromagnetic field Green function of the form

$$g(\mathbf{r}, \mathbf{r}_A, \omega) = g_0(\mathbf{r}, \mathbf{r}_A, \omega) - \frac{R_{cn}}{(2\pi)^2} \sum_{p=-\infty}^{\infty} e^{ip\varphi} \int_C \frac{\beta(\omega) v^2 I_p^2(vR_{cn}) K_p(vr_A) K_p(vr)}{1 + \beta(\omega) v^2 R_{cn} I_p(vR_{cn}) K_p(vR_{cn})} e^{ihz} dh, \quad (110)$$

where $r_A \geq r > R_{cn}$. One may show in a similar way that the function $g(\mathbf{r}, \mathbf{r}_A, \omega)$ for $r \leq r_A < R_{cn}$ is obtained from Eq. (110) by means of a simple symbol replacement $I_p \leftrightarrow K_p$ in the numerator of the integrand.

Knowing $g(\mathbf{r}, \mathbf{r}_A, \omega)$, one can easily calculate from Eq. (100) the components of the electromagnetic field Green tensor ${}^\perp G_{\alpha z}(\mathbf{r}, \mathbf{r}_A, \omega)$ and, consequently, ${}^\perp G_{zz}(\mathbf{r}, \mathbf{r}_A, \omega)$ and ${}^\parallel G_{zz}(\mathbf{r}, \mathbf{r}_A, \omega)$ defined by Eqs. (95) and (97), respectively, which we actually need.

(b) Local photonic DOS near a single-wall carbon nanotube

Using Eqs. (95), (97), (91) and the property $g(\mathbf{r}, \mathbf{r}_A, \omega) = g(\mathbf{r}_A, \mathbf{r}, \omega)$ which is obvious from Eqs. (99) and (110), it is not difficult to prove that

$${}^\perp G_{zz}^\perp(\mathbf{r}_A, \mathbf{r}_A, \omega) = {}^\perp G_{zz}(\mathbf{r}_A, \mathbf{r}_A, \omega), \quad (111)$$

$${}^\parallel G_{zz}^\parallel(\mathbf{r}_A, \mathbf{r}_A, \omega) = {}^\parallel G_{zz}(\mathbf{r}_A, \mathbf{r}_A, \omega), \quad (112)$$

$${}^\perp G_{zz}^\parallel(\mathbf{r}_A, \mathbf{r}_A, \omega) = 0, \quad (113)$$

whereupon, making use of the definition (34) and Eqs. (36)–(41), one arrives for $r_A > R_{cn}$ at the \mathbf{r}_A -dependent transverse and longitudinal local photonic DOS functions of the form

$$\bar{\xi}^\perp(\mathbf{r}_A, \omega) = \frac{3R_{cn}}{2\pi k^3} \text{Im} \sum_{p=-\infty}^{\infty} \int_C \frac{dh \beta(\omega) v^4 I_p^2(vR_{cn}) K_p^2(vr_A)}{1 + \beta(\omega) v^2 R_{cn} I_p(vR_{cn}) K_p(vR_{cn})}, \quad (114)$$

$$\bar{\xi}^\parallel(\mathbf{r}_A, \omega) = \frac{3R_{cn}}{2\pi k^3} \text{Im} \sum_{p=-\infty}^{\infty} \int_C \frac{dh \beta(\omega) h^2 v^2 I_p^2(vR_{cn}) K_p^2(vr_A)}{1 + \beta(\omega) v^2 R_{cn} I_p(vR_{cn}) K_p(vR_{cn})}. \quad (115)$$

Here, the sign in front of Eq. (115) has been changed to be positive. This reflects the fact that the right-hand sides of Eqs. (96) and (98) are of opposite signs. As a consequence, partial solutions of the corresponding homogeneous equations should be taken to have opposite signs as well. This yields a correct (positive) sign of the longitudinal local photonic DOS which, along with the transverse local photonic DOS, must be a positively defined function. For $r_A < R_{cn}$, Eqs. (114) and (115) should be modified by the replacement $r_A \leftrightarrow R_{cn}$ in the Bessel function arguments

in the numerators of the integrands. In dimensionless variables (44), after the transformation of the integration variable $h = ky$, these equations are rewritten to give Eqs. (42) and (43).

(c) Proof of Eqs. (32) and (33)

Based upon the properties (111)–(113), one can easily prove Eqs. (32) and (33) for the dipole interaction matrix elements. The proof of Eq. (32) is straightforward. In view of Eq. (30), one has

$$\begin{aligned} \int d\mathbf{R} |g^{\perp(\parallel)}(\mathbf{r}_A, \mathbf{R}, \omega)|^2 &= \pi \hbar \omega \frac{16\omega_A^2 d_z^2}{c^4} \int d\mathbf{R} \operatorname{Re} \sigma_{zz}(\mathbf{R}, \omega) \\ &\times {}^{\perp(\parallel)}G_{zz}(\mathbf{r}_A, \mathbf{R}, \omega) {}^{\perp(\parallel)}G_{zz}(\mathbf{r}_A, \mathbf{R}, \omega)^*. \end{aligned} \quad (116)$$

Using further the integral relationship

$$\operatorname{Im} G_{\alpha\beta}(\mathbf{r}, \mathbf{r}', \omega) = \frac{4\pi}{c} k \int d\mathbf{R} \operatorname{Re} \sigma_{zz}(\mathbf{R}, \omega) G_{\alpha z}(\mathbf{r}, \mathbf{R}, \omega) G_{\beta z}(\mathbf{r}', \mathbf{R}, \omega)^* \quad (117)$$

[which is nothing but a particular 2D case of a general integral relationship proven for any 3D electromagnetic field Green tensor in Ref. [13], with Eq. (4) taken into account], one obtains for the right-hand side of Eq. (116)

$$\hbar \frac{4\omega_A^2 d_z^2}{c^2} \operatorname{Im} {}^{\perp(\parallel)}G_{zz}^{\perp(\parallel)}(\mathbf{r}_A, \mathbf{r}_A, \omega),$$

whereupon using Eqs. (34) and (36), one arrives at Eq. (32).

The proof of Eq. (33) is based upon Eq. (32). In view of this equation, the right-hand side of Eq. (33) takes the form

$$\begin{aligned} \int d\mathbf{R} |g^{(\pm)}(\mathbf{r}_A, \mathbf{R}, \omega)|^2 &= \frac{(\hbar\omega_A)^2}{2\pi\omega^2} \Gamma_0(\omega) \left[\xi^{\perp}(\mathbf{r}_A, \omega) + \left(\frac{\omega}{\omega_A} \right)^2 \xi^{\parallel}(\mathbf{r}_A, \omega) \right] \\ &\pm \frac{\omega}{\omega_A} 2\operatorname{Re} \int d\mathbf{R} g^{\perp}(\mathbf{r}_A, \mathbf{R}, \omega) g^{\parallel}(\mathbf{r}_A, \mathbf{R}, \omega)^*, \end{aligned} \quad (118)$$

where the last item can be further rewritten in terms of Eqs. (30), (31) and (117) to give

$$\hbar \frac{8\omega\omega_A d_z^2}{c^2} \operatorname{Im} {}^{\perp}G_{zz}^{\parallel}(\mathbf{r}_A, \mathbf{r}_A, \omega),$$

which is zero, according to Eq. (113). Thus, one arrives at Eq. (33).

C Relation of Eq. (70) with the Casimir–Polder formula

In deriving an 'infinitely conducting plane' result (the Casimir-Polder formula [60]) from our theory, we will follow a general line of the work by Marvin and Toigo [74] who did the same within the framework of their linear response theory.

We start with our weak-coupling-regime equation (74). First of all one has to simplify the local DOS functions $\bar{\xi}^{\perp(\parallel)}(\mathbf{r}_A, x)$ in this equation by putting $\bar{\sigma}_{zz} \rightarrow \infty$. From Eqs. (42) and (43), one has then for $r_A > R_{cn}$

$$\left\{ \begin{array}{l} \bar{\xi}^{\perp}(\mathbf{r}_A, x) \\ \bar{\xi}^{\parallel}(\mathbf{r}_A, x) \end{array} \right\} = \frac{3}{\pi} \text{Im} \int_0^{\infty} dy \left\{ \begin{array}{l} y^2 - 1 - i\varepsilon \\ y^2 \end{array} \right\} \times \sum_{p=-\infty}^{\infty} \frac{K_p^2[\sqrt{y^2 - 1 - i\varepsilon} u(r_A)x] I_p[\sqrt{y^2 - 1 - i\varepsilon} u(R_{cn})x]}{K_p[x\sqrt{y^2 - 1 - i\varepsilon} u(R_{cn})x]}, \quad (119)$$

where ε is an infinitesimal positive constant which is necessary to correctly envelope the branch points of the integrand in integrating over y .

The next step is taking a large radius limit in Eq. (119). This can be done by using the relationship

$$\lim_{\substack{a \rightarrow \infty \\ b \rightarrow \infty \\ (a-b = \text{const})}} \sum_{n=-\infty}^{\infty} \frac{K_n^2(a) I_n(b)}{K_n(b)} = K_0[2(a-b)]$$

proved in Ref. [74]. One has

$$\left\{ \begin{array}{l} \bar{\xi}^{\perp}(\mathbf{r}_A, x) \\ \bar{\xi}^{\parallel}(\mathbf{r}_A, x) \end{array} \right\} = \frac{3}{\pi} \text{Im} \int_0^{\infty} dy \left\{ \begin{array}{l} y^2 - 1 - i\varepsilon \\ y^2 \end{array} \right\} K_0[2\mu x \sqrt{y^2 - 1 - i\varepsilon}], \quad (120)$$

where $\mu = 2\gamma_0 l / \hbar c$ with $l = r_A - R_{cn}$ being the atom-surface distance. The integration variable y in this equation contains implicit frequency dependence. Indeed, comparing dimensionless equations (42), (43) with (114), (115), one can see that $y = h/k = h(c/\omega) = h(c\hbar/2\gamma_0 x)$. For the following it makes sense to extract this frequency dependence by the substitution $y = \lambda/x$ with the dimensionless $\lambda = h(c\hbar/2\gamma_0)$. The result takes the form

$$\bar{\xi}^{\perp(\parallel)}(\mathbf{r}_A, x) = \frac{3}{2i\pi x} \left\{ f^{\perp(\parallel)}(\mathbf{r}_A, x) - f^{\perp(\parallel)*}(\mathbf{r}_A, x) \right\} \quad (121)$$

with

$$\left\{ \begin{array}{l} f^{\perp}(\mathbf{r}_A, x) \\ f^{\parallel}(\mathbf{r}_A, x) \end{array} \right\} = \int_0^{\infty} d\lambda \left\{ \begin{array}{l} (\lambda/x)^2 - 1 - i\varepsilon \\ (\lambda/x)^2 \end{array} \right\} K_0[2\mu x \sqrt{(\lambda/x)^2 - 1 - i\varepsilon}]. \quad (122)$$

Substituting Eq. (121) into Eq. (74), one has

$$\begin{aligned} \varepsilon_{vw}(\mathbf{r}_A) = & \frac{3x_A}{4i\pi^2} \left\{ \int_0^\infty \frac{dx \tilde{\Gamma}_0(x)}{(x_A+x)x^2} \left[f^\perp(\mathbf{r}_A, x) - \frac{x}{x_A} f^\parallel(\mathbf{r}_A, x) \right] \right. \\ & \left. - \int_0^{-\infty} \frac{dx \tilde{\Gamma}_0(x)}{(x_A-x)x^2} \left[f^\perp(\mathbf{r}_A, -x)^* + \frac{x}{x_A} f^\parallel(\mathbf{r}_A, -x)^* \right] \right\}. \end{aligned} \quad (123)$$

Here, in the second item, the change of the integration variable from x to $-x$ has been made and it has been taken into account that $\tilde{\Gamma}_0(-x) = -\tilde{\Gamma}_0(x)$. Noting further that both integrands in Eq. (123) do not have poles in the upper complex half plane, one may rotate the integration path of the first and the second integral by $\pi/2$ and by $-\pi/2$, respectively. Then, both integrals become the integrals over the positive imaginary axis of the complex plane and Eq. (123) takes the form

$$\begin{aligned} \varepsilon_{vw}(\mathbf{r}_A) = & \frac{3x_A}{4i\pi^2} \left\{ \int_0^{i\infty} \frac{dz \tilde{\Gamma}_0(z)}{(x_A+z)z^2} \left[f^\perp(\mathbf{r}_A, z) - \frac{z}{x_A} f^\parallel(\mathbf{r}_A, z) \right] \right. \\ & \left. - \int_0^{i\infty} \frac{dz \tilde{\Gamma}_0(z)}{(x_A-z)z^2} \left[f^\perp(\mathbf{r}_A, -z)^* + \frac{z}{x_A} f^\parallel(\mathbf{r}_A, -z)^* \right] \right\}. \end{aligned} \quad (124)$$

Making further the change of the integration variable from z to iu with real non-negative u , one arrives at

$$\begin{aligned} \varepsilon_{vw}(\mathbf{r}_A) = & \frac{3x_A}{4\pi^2} \left\{ - \int_0^\infty \frac{du \tilde{\Gamma}_0(iu)}{(x_A+iu)u^2} \left[f^\perp(\mathbf{r}_A, iu) - \frac{iu}{x_A} f^\parallel(\mathbf{r}_A, iu) \right] \right. \\ & \left. + \int_0^\infty \frac{du \tilde{\Gamma}_0(iu)}{(x_A-iu)u^2} \left[f^\perp(\mathbf{r}_A, -iu)^* + \frac{iu}{x_A} f^\parallel(\mathbf{r}_A, -iu)^* \right] \right\}. \end{aligned} \quad (125)$$

Here, the functions $f^{\perp(\parallel)}(\mathbf{r}_A, iu)$ have the following explicit form

$$\begin{Bmatrix} f^\perp(\mathbf{r}_A, iu) \\ f^\parallel(\mathbf{r}_A, iu) \end{Bmatrix} = -u \int_1^\infty d\eta \begin{Bmatrix} \eta^3 / \sqrt{\eta^2 - 1} \\ \eta \sqrt{\eta^2 - 1} \end{Bmatrix} K_0(2\mu u \eta) \quad (126)$$

obtained from Eq. (122) after the change of the integration variable by the subsequent substitutions $x = iu$ and $\eta^2 = \lambda^2/u^2 + 1$. The functions $f^{\perp(\parallel)}(-iu)^* = f^{\perp(\parallel)}(iu)$ as a consequence of a general property $K_\nu(z)^* = K_\nu(z^*)$ [56]. Substituting Eq. (126) into Eq. (125) and making allowance for the fact that $\tilde{\Gamma}_0(iu) = -i\tilde{\Gamma}_0(u)$, one further has

$$\varepsilon_{vw}(\mathbf{r}_A) = -\frac{3x_A}{2\pi^2} \int_0^\infty \frac{du \tilde{\Gamma}_0(u)}{x_A^2 + u^2} \int_1^\infty d\eta \eta \left(\sqrt{\eta^2 - 1} + \frac{\eta^2}{\sqrt{\eta^2 - 1}} \right) K_0(2\mu u \eta), \quad (127)$$

which upon the substitution $\eta^2 = \rho$ becomes

$$\varepsilon_{vw}(\mathbf{r}_A) = -\frac{3x_A}{4\pi^2} \int_0^\infty \frac{du \tilde{\Gamma}_0(u)}{x_A^2 + u^2} \int_1^\infty d\rho \left(\sqrt{\rho-1} + \frac{\rho}{\sqrt{\rho-1}} \right) K_0(2\mu u \sqrt{\rho}). \quad (128)$$

In Eq. (128), the first integral over ρ is taken exactly by means of the relationship [75]

$$\int_1^\infty d\rho \sqrt{\rho-1} K_0(a\sqrt{\rho}) = \sqrt{\frac{2\pi}{a^3}} K_{3/2}(a) \xrightarrow{a \rightarrow \infty} \frac{\pi}{a^3} (1+a) e^{-a}$$

and the second one – by making a large argument series expansion of the integrand and its subsequent termwise integration. This, upon returning back to dimensional variables by means of Eqs. (69) and using the definition (see, e.g., [49, 71])

$$\alpha_{zz}(iu) = \frac{2}{\hbar} \frac{d_z^2 \omega_A}{\omega_A^2 - (iu)^2}$$

for the polarizability tensor zz -component of the two-level system, finally yields

$$E_{vw}(\mathbf{r}_A) \approx -\frac{\hbar}{8\pi l^3} \int_0^\infty du \alpha_{zz}(iu) \left[1 + 2\frac{u}{c} l + 2\left(\frac{u}{c}\right)^2 l^2 \right] e^{-2(u/c)l}.$$

This is the half of the well-known Casimir-Polder result for the vdW energy of an atom near an infinitely conducting plane (see Refs. [60, 74]), in agreement with the fact that our model of the atom-electromagnetic-field interactions in the presence of a nanotube only takes the longitudinal (along the nanotube axis, or, equivalently, parallel to the plane in the large nanotube radius limit) atomic dipole orientation into account. Another half of the Casimir-Polder vdW energy would come from the transverse (perpendicular to the plane) atomic dipole orientation which we have neglected.

References

- [1] Dresselhaus M.S., Dresselhaus G., and Eklund P.C. *Science of Fullerenes and Carbon Nanotubes*, Academic Press, New York, 1996.
- [2] Dai H. *Surf. Sci.* **500**, 218 (2002).
- [3] Baughman R.H., Zakhidov A.A., and de Heer W.A. *Science* **297**, 787 (2002).
- [4] Duclaux L. *Carbon* **40**, 1751 (2002).
- [5] Jeong G.-H., Farajian A.A., Hatakeyama R., Hirata T., Yaguchi T., Tohji K., Mizuseki H., and Kawazoe Y. *Phys. Rev. B* **68**, 075410 (2003).
- [6] Shimoda H., Gao B., Tang X.P., Kleinhammes A., Fleming L., Wu Y., and Zhou O. *Phys. Rev. Lett.* **88**, 015502 (2002).

- [7] Calbi M.M., Cole M.W., Gatica S.M., Bojan M.J., and Stan G. *Rev. Mod. Phys.* **73**, 857 (2001).
- [8] Purcell E.M. *Phys. Rev.* **69**, 681 (1946).
- [9] Rarity J.D. and Weisbuch C. *Microcavities and Photonic Bandgaps: Physics and Applications*, NATO ASI Series, Vol. E324, Kluwer, Dordrecht, 1996.
- [10] Pelton M. and Yamamoto Y. *Phys. Rev. A* **59**, 2418 (1999).
- [11] Vučković J., Fattal D., Santori C., Solomon G.S., and Yamamoto Y. *Appl. Phys. Lett.* **82**, 3596 (2003).
- [12] Dung H.T., Knöll L., and Welsch D.-G. *Phys. Rev. A* **62**, 053804 (2000); *ibid.* **64**, 013804 (2001) [and refs. therein].
- [13] Knöll L., Scheel S., and Welsch D.-G. in: *Coherence and Statistics of Photons and Atoms*, edited by Peřina J., Wiley, New York, 2001 [see also *quant-ph/0006121* (26 Jun 2003)].
- [14] Buck J.R. and Kimble H.J. *Phys. Rev. A* **67**, 033806 (2003).
- [15] Klimov V.V. and Ducloy M. *Phys. Rev. A* **69**, 013812 (2004).
- [16] Florescu M. and John S. *Phys. Rev. A* **64**, 033801 (2001).
- [17] Sugawara M. *Phys. Rev. B* **51**, 10743 (1995).
- [18] Schniepp H. and Sandoghdar V. *Phys. Rev. Lett.* **89**, 257403 (2002).
- [19] Reithmaier J.P., Sek G., Löffler A., Hoffman C., Kuhn S., Reitzenstein S., Keldysh L.V., Kulakovskii V.D., Reinecke T.L., and Forchel A. *Nature*, **432**, 197 (2004).
- [20] Gayral B., Gérard J.-M., Sermage B., Lemaître A., and Dupuis C. *Appl. Phys. Lett.* **78**, 2828 (2001).
- [21] Peter E., Senellart P., Martrou D., Lemaître A., Hours J., Gérard J.M., and Bloch J. *quant-ph/0411076* (3 Dec 2004).
- [22] Petrov E.P., Bogomolov V.N., Kalosha I.I., and Gaponenko S.V. *Phys. Rev. Lett.* **81**, 77 (1998).
- [23] Yoshie T., Scherer A., Hendrikson J., Khitrova G., Gibbs H.M., Rupper G., Ell C., Shchekin O.B., and Deppe D.G. *Nature*, **432**, 200 (2004).
- [24] Kress A., Hofbauer F., Reinelt N., Krener H.J., Meyer R., Böhm G., and Finley J.J. *quant-ph/0501013* (4 Jan 2005).

- [25] Allen L. and Eberly J.H. *Optical Resonance and Two-Level Atoms*, Wiley, New York, 1975.
- [26] Bondarev I.V., Slepyan G.Ya., and Maksimenko S.A. *Phys. Rev. Lett.* **89**, 115504 (2002).
- [27] Bondarev I.V. and Lambin Ph. *Phys. Lett. A* **328**, 235 (2004).
- [28] Bondarev I.V. and Lambin Ph. *Phys. Rev. B* **70**, 035407 (2004).
- [29] Buhmann S.Y., Dung H.T., and Welsch D.-G. *J. Opt. B: Quantum Semiclass. Opt.* **6**, S127 (2004).
- [30] Buhmann S.Y., Dung H.T., Knöll L., and Welsch D.-G. *quant-ph/0403128* (17 Mar 2004).
- [31] Zhao J., Buldum A., Han J., and Lu J.P. *Nanotechnology* **13** 195 (2002).
- [32] Zhang X.R., Cao D.P., and Chen J.F. *J. Phys. Chem. B* **107**, 4942 (2003).
- [33] Han S.S. and Lee H.M. *Carbon* **42**, 2169 (2004).
- [34] Dag S., Gulseren O., Yildirim T., and Ciraci S. *Phys. Rev. B* **67**, 165424 (2003).
- [35] Girifalco L.A. and Hodak M. *Phys. Rev. B* **65**, 125404 (2002).
- [36] London F. *Zs. f. Physik* **60**, 491 (1930).
- [37] Williams K.A. and Eklund P.C. *Chem. Phys. Lett.* **320**, 352 (2000).
- [38] Ulbricht H., Moos G., and Hertel T. *Phys. Rev. B* **66**, 075404 (2002).
- [39] Slepyan G.Ya., Maksimenko S.A., Lakhtakia A., Yevtushenko O., and Gusakov A.V. *Phys. Rev. B* **60**, 17136 (1999).
- [40] Benedict L.X., Louie S.G., and Cohen M.L. *Phys. Rev. B* **52**, 8541 (1995).
- [41] Tasaki S., Maekawa K., and Yamabe T. *Phys. Rev. B* **57**, 9301 (1998).
- [42] Jorio A., Souza Filho A.G., Brar V.W., Swan A.K., Ünlü M.S., Goldberg B.B., Righi A., Hafner J.H., Lieber C.M., Saito R., Dresselhaus G., and Dresselhaus M.S. *Phys. Rev. B* **65**, 121402(R) (2002).
- [43] Li Z.M., Tang Z.K., Liu H.J., Wang N., Chan C.T., Saito R., Okada S., Li G.D., Chen J.S., Nagasawa N., and Tsuda S. *Phys. Rev. Lett.* **87**, 127401 (2001).
- [44] Marinopoulos A.G., Reining L., Rubio A., and Vast N. *Phys. Rev. Lett.* **91**, 046402 (2003).

- [45] Weisbuch C., Nishioka M., Ishikawa A., and Arakawa Y. *Phys. Rev. Lett.* **69**, 3314 (1992).
- [46] Dini D., Köhler R., Tredicucci A., Biasiol G., and Sorba L. *Phys. Rev. Lett.* **90**, 116401 (2003).
- [47] Bondarev I.V. and Lambin Ph. *Solid State Commun. A* **132**, 203 (2004).
- [48] Bondarev I.V. and Lambin Ph. *cond-mat/0410216* (8 Oct 2004).
- [49] Davydov A.S. *Quantum Mechanics*, Pergamon, New York, 1976.
- [50] Vogel W., Welsch D.-G., and Wallentowitz S. *Quantum Optics: an Introduction*, Wiley-VCH, New York, 2001.
- [51] Jackson J.D. *Classical Electrodynamics*, Wiley, New York, 1975.
- [52] Abrikosov A.A., Gorkov L.P., and Dzyaloshinski I.E. *Methods of Quantum Field Theory in Statistical Physics*, Dover, New York, 1975.
- [53] Barnett S.M., Huttner B., and Loudon R. *Phys. Rev. Lett.* **68**, 3698 (1992).
- [54] Agarwal G.S. *Phys. Rev. A* **12**, 1475 (1975).
- [55] Wallace P.R. *Phys. Rev.* **71**, 622 (1947).
- [56] Abramovitz M. and Stegun I.A. (Eds) *Handbook of Mathematical Functions*, Dover, New York, 1972.
- [57] Henrard L. and Lambin Ph. *J. Phys. B* **29**, 5127 (1996).
- [58] Heitler W. *The Quantum Theory of Radiation*, Oxford, London, 1954.
- [59] Watson, G.N. *Theory of Bessel Functions*, Cambridge University Press, Cambridge, 1922.
- [60] Casimir H.B.G. and Polder D. *Phys. Rev.* **73**, 360 (1948).
- [61] Lide D.R. (Editor-in-Chief) *Handbook of Chemistry and Physics*, CRC Press, New York, 1999.
- [62] Masenelli-Varlot K., McRae E., and Dupont-Pavlovsky N. *Appl. Surf. Sci.* **196**, 209 (2002).
- [63] Haroche S. and Kleppner D. *Phys. Today* **42**, No. 1, 24 (1989).
- [64] Vučković J. and Yamamoto Y. *Appl. Phys. Lett.* **82**, 2374 (2003).
- [65] Asano T. and Noda S. *Nature* **429**, 6988 (2004).

- [66] Raimond J.M., Brune M., and Haroche S. *Rev. Mod. Phys.* **73**, 565 (2001).
- [67] Zrenner A., Beham E., Stufler S., Findeis F., Bichler M., and Abstreiter G. *Nature* **418**, 612 (2002).
- [68] Li X., Wu Y., Steel D., Gammon D., Stievater T.H., Katzer D.S., Park D., Piermarocchi C., and Sham L.J. *Science* **301**, 809 (2003).
- [69] Bondarev I.V., Maksimenko S.A., Slepyan G.Ya., Krestnikov I.L., and Hoffmann A. *Phys. Rev. B* **68**, 073310 (2003).
- [70] Dung H.T., Scheel S., Welsch D.-G., and Knoll L. *J. Opt. B: Quantum Semi-class. Opt.* **4**, S169 (2002).
- [71] Agarwal G.S. and Dutta Gupta S. *Phys. Rev. A* **57**, 667 (1998).
- [72] Dung H.T., Knöll L., and Welsch D.-G. *Phys. Rev. A* **66**, 063810 (2002).
- [73] Dalton B.J. and Garraway B.M. *Phys. Rev. A* **68**, 033809 (2003).
- [74] Marvin A.M. and Toigo F. *Phys. Rev. A* **25**, 782 (1982).
- [75] Gradshteyn I.S. and Ryzhik I.M. *Tables of Integrals, Series and Products*, Academic, New York, 1965.